Enhanced Orthogonal Frequency Division Multiplexing With Index Modulation

Miaowen Wen, *Member, IEEE*, Binbin Ye, Ertugrul Basar, *Senior Member, IEEE*, Qiang Li, and Fei Ji, *Member, IEEE*

***Abstract*— Index modulation concept has attracted considerable research interest in the past few years. As a realization of index modulation in the frequency domain, orthogonal frequency division multiplexing with index modulation (OFDM-IM) has recently been proposed, which conveys information bits through both the subcarrier activation patterns and the amplitude phase modulation constellation points. This paper proposes two enhanced OFDM-IM schemes aimed at achieving higher spectral efficiency and diversity gain, respectively. The first one, termed OFDM with hybrid in-phase/quadrature index modulation (OFDM-HIQ-IM), explores the I- and Q- dimensions jointly for index modulation, allowing transmission of more index modulation bits in each subcarrier group. The second one, termed linear constellation precoded OFDM-IQ-IM (LP-OFDM-IQ-IM), spreads information symbols across two adjacent active subcarriers through linear constellation precoding to harvest additional diversity gain. By maximizing the minimum squared Euclidean distance, two different realizations of LP-OFDM-IQ-IM are derived, which leads to a rotated and a diamond-shaped constellation, respectively. The proposed OFDM-HIQ-IM and LP-OFDM-IQ-IM, as revealed by both theoretical analyses and computer simulations, enable low-complexity detection and exhibit superior error rate performance over the existing OFDM-IM schemes.**

***Index Terms*— Coordinate interleaving, index modulation, in-phase/quadrature, linear constellation precoding, log-likelihood ratio, OFDM.**

I. Introduction

INDEX modulation (IM) is a recently-emerging concept, which, as its name suggests, refers to a category of modulation techniques that rely on the index(es) of some medium to modulate information bits, where the medium can be either actual, such as antenna and frequency carrier, or virtual, such as space-time matrix, antenna activation order, and virtual parallel channels [1], [2]. The information bits carried by the index(es) generally consume little or even no power, making IM techniques very competitive candidates for the fifth generation (5G) wireless networks that aim at both high spectral efficiency (SE) and energy efficiency (EE) [2].

Spatial modulation (SM) [3], which belongs to the multiple-input multiple-output (MIMO) family, is a famous representative of IM applied to the space domain. In SM, a single antenna is activated to transmit an M-ary modulated symbol, whose index is involved in the process of information conveying. Owing to the requirement of a single radio frequency (RF) chain, the EE of SM is shown to potentially outperform that of conventional MIMO systems [4], [5]. However, the random activation of a single antenna in SM limits the SE of the system and the diversity gain to the receiver side. To improve the SE, a natural way is to activate more antennas and use the antenna combination for indexing. Such idea has been realized by the so-termed generalized spatial modulation (GSM), in which multiple active antennas can transmit only one [6] or multiple modulated symbols [7] depending on the configuration of RF chains. Another effective way to improve the SE is to expand the spatial constellation domain to a new dimension by utilizing both in-phase (I-) and quadrature (Q-) components. This scheme, called quadrature spatial modulation (QSM), transmits an additional base-two logarithm of the number of transmit antennas bits without adding any new RF chain [8]. Naturally, by allowing multiple RF chains to transmit multiple modulated symbols, the SE can be further improved with QSM [9]. Besides the aforementioned two schemes, the enhanced spatial modulation (ESM) scheme can also improve the SE by using multiple distinguishable signal constellations [10]. On the other hand, to improve the diversity gain, many efficient schemes have been proposed, including the space-time block coded spatial modulation (STBC-SM) [11] and the coordinate interleaved spatial modulation (CI-SM) [12]. STBC-SM uses the Alamouti code [13] as a basic transmission structure to achieve additional transmit diversity order whilst CI-SM applies the coordinate interleaved orthogonal design (CIOD) principle, which was originally proposed for communications over single-antenna channel [14], [15] and MIMO channels [16]–[18], to achieve signal-space modulation diversity. More related studies on SM can be found in the recent surveys of [19], [20].

Manuscript received October 18, 2016; revised February 17, 2017 and April 30, 2017; accepted May 3, 2017. Date of publication May 16, 2017; date of current version July 10, 2017. This work was supported in part by the National Natural Science Foundation of China under Grant 61431005 and Grant 61501190, in part by the Natural Science Foundation of Guangdong Province under Grant 2016A030308006, and in part by the open research fund of National Mobile Communications Research Laboratory, Southeast University under Grant 2017D08. The associate editor coordinating the review of this paper and approving it for publication was E. A. Jorswieck. *(Corresponding author: Miaowen Wen.)*

M. Wen is with the School of Electronic and Information Engineering, South China University of Technology, Guangzhou 510640, China, and also with the National Mobile Communications Research Laboratory, Southeast University, Nanjing 210096, China (e-mail: eemwwen@scut.edu.cn).

B. Ye, Q. Li, and F. Ji are with the School of Electronic and Information Engineering, South China University of Technology, Guangzhou 510640, China (e-mail: yebinbin_13@163.com; eeqiangli@mail.scut.edu.cn; eefeiji@scut.edu.cn).

E. Basar is with the Faculty of Electrical and Electronics Engineering, Istanbul Technical University, Istanbul 34469, Turkey (e-mail: basarer@itu.edu.tr).

Color versions of one or more of the figures in this paper are available online at http://ieeexplore.ieee.org.

Digital Object Identifier 10.1109/TWC.2017.2702618

1536-1276 © 2017 IEEE. Personal use is permitted, but republication/redistribution requires IEEE permission.
See http://www.ieee.org/publications_standards/publications/rights/index.html for more information.

Orthogonal frequency division multiplexing with index modulation (OFDM-IM), which is a modification of OFDM, is a promising frequency-domain IM technique [2]. Similar to GSM, OFDM-IM activates a subset of subcarriers to transmit M-ary modulated symbols and uses the subcarrier activation patterns (SAPs) to convey additional information. This principle originally appeared in 1999 [21], which is motivated by the parallel combinatory spread spectrum concept. As the development of SM, OFDM-IM has been also developed. The first scheme that exploits a similar idea is called subcarrier index modulation OFDM (SIM-OFDM) [22], in which half of the subcarriers are activated according to the incoming information bits and some of the other subcarriers are dedicated to control signaling. To solve the underlying error propagation problem in SIM-OFDM, an enhanced SIM-OFDM scheme is later proposed in [23], which uses one bit to control two adjacent subcarriers such that only one subcarrier is activated at a time. The limitation on the number of active subcarriers is relaxed in [24], where the proposed new scheme is coined as what we know OFDM-IM. After the emergence of [24], OFDM-IM has started to receive widespread attention from the research community. Similar to classical OFDM, OFDM-IM is able to exhibit single-symbol decoding complexity when employing the log-likelihood ratio (LLR) [24] or low-complexity maximum-likelihood (ML) [25] detection. Performance comparison with classical OFDM has been made in the literature for both uncoded and coded scenarios, where the available results show that OFDM-IM enjoys lower bit error rate (BER) [24], higher achievable rate [26], and higher EE [27], [28]. Moreover, since only partial subcarriers are active, OFDM-IM has the potential to suppress the inter-carrier interference [29], which usually arises in OFDM systems, and can be applied to communication applications suffering from severe Doppler effects, such as underwater acoustic communications [30].

Similar to the case of SM, the SE and diversity issues exist in OFDM-IM. So far, a great deal of work have been performed to explore the SE issue. In [31], OFDM with generalized index modulation (OFDM-GIM) is proposed, where the number of active subcarriers is variable and more SAPs are encoded for indexing. Motivated by the idea of QSM, OFDM with in-phase/quadrature index modulation (OFDM-IQ-IM) is designed, which performs OFDM-IM on the I- and Q- components independently, doubling the number of IM bits [25], [31]. Moreover, it is reported that under an SE of 2 bps/Hz, OFDM-IQ-IM demonstrates more than 6dB and 3dB signal-to-noise ratio (SNR) gains over classical OFDM and OFDM-IM, respectively [25]. Unlike the aforementioned two schemes, which focus on the enlargement of the index domain, the recently-emerging dual-mode index modulation aided OFDM (DM-OFDM) improves the SE by ensuring the increase of the number of ordinary modulation bits. The improvement is achieved by dividing all subcarriers into two groups and modulating the subcarriers within groups with two distinguishable constellation alphabets [32]. In [33] and [34], a direct combination of OFDM-IM with MIMO transmission techniques, which is called MIMO-OFDM-IM, is proposed to obtain a linear increase of the SE, while sequential Monte-Carlo based low-complexity near-ML detection algorithms are proposed for MIMO-OFDM-IM in [35]. Alternative to this direct combination, generalized space-and-frequency index modulation (GSFIM) improves the SE by activating a group of transmit antennas according to partial information bits and selecting the active space-frequency elements at the active transmit antennas according to the remaining information bits [36]. On the other hand, different ways have been used to explore the diversity issue. Instead of localized subcarrier grouping, the interleaved based version is suggested for OFDM-IM to obtain frequency diversity [26], [37], [38]. In [39], the CIOD is applied to two complex modulated symbols carried on an active subcarrier pair, which improves the transmit diversity of OFDM-IM from unity to two. By combining the Alamouti code and MIMO-OFDM-IM, an additional diversity gain is obtained by the space-frequency coded index modulation (SFC-IM) scheme [40].

Against the background, we propose two new schemes to enhance the performance of OFDM-IM with a focus on SE and diversity gain, respectively. Their principles and advantages are summarized as follows.

- The first proposed scheme is called OFDM with hybrid in-phase/quadrature index modulation (OFDM-HIQ-IM), which selects the elements from the grid formed jointly by the I- and Q- dimensions for indexing. The idea is motivated from the property that the IM bits have a stronger protection than the ordinary modulation bits and from the deficiency of OFDM-IQ-IM that when the number of SAPs is not equal to an integer power of two, a considerable portion of SAPs have to be discarded due to the independent indexing of I- and Q- components. However, we notice that involving all possible elements for indexing will not necessarily improve the BER performance since some active elements may experience the same fading, which results in a loss of frequency diversity. To solve this problem, OFDM-HIQ-IM only includes those with the equal number of I- and Q- components for indexing, allowing the transmission of one more IM bit in each subcarrier group than OFDM-IQ-IM in most cases. Both LLR and low-complexity ML detectors that exhibit near-optimum performance, are designed for OFDM-HIQ-IM. An asymptotically tight upper bound on the BER and the analysis for the achievable rate of OFDM-HIQ-IM systems are also provided.
- The second proposed scheme, which is called linear constellation precoded OFDM-IQ-IM (LP-OFDM-IQ-IM), is motivated from the linear constellation precoding (LCP) technique, which was originally proposed for OFDM systems to achieve the maximum diversity gain and includes the CIOD as its special case [41], [42]. To the best of our knowledge, only [43] attempts to employ the LCP to enhance the diversity performance of an IM system, namely SM-OFDM. However, a direct application of this method to OFDM-IM related systems may be not efficient since in those systems, the minimum squared Euclidean distance of the transmitted signal set additionally depends on IM. Specially, in LP-OFDM-IQ-IM, the subcarrier activation effect is considered in the design and the LCP

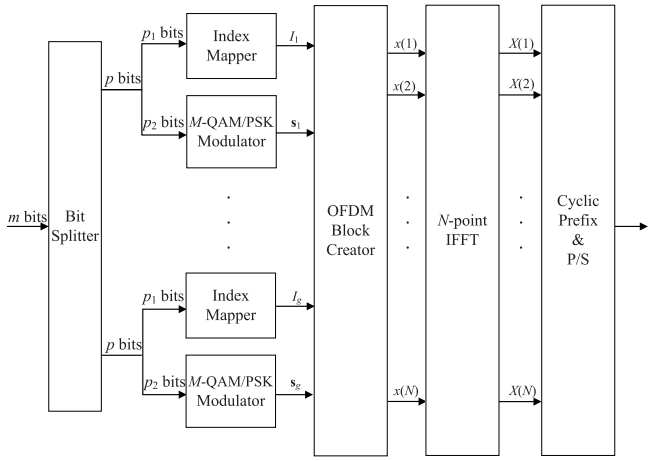

Fig. 1. Block diagram of the OFDM-IM transmitter.

applies to the I- and Q- components of OFDM-IM signals simultaneously. By maximizing the minimum squared Euclidean distance, two different precoding methods that resort to the constellation rotation and constellation compression, respectively, are derived, harvesting a diversity order of two.

The rest of this paper is outlined as follows. Section II gives a brief review of OFDM-IM. The transceiver structure and theoretical analyses, including the BER and achievable rate performance, of OFDM-HIQ-IM are presented in Section III. Section IV describes the LCP design for LP-OFDM-IQ-IM. Computer simulation results and comparisons are given in Section V. Finally, Section VI concludes the paper.[1]

II. OFDM-IM Revisited

The block diagram of the OFDM-IM transmitter is redrawn from [24] in Fig. 1. The total OFDM subcarriers have a count of N and are divided into g groups, each consisting of $N/g = n$ subcarriers. We consider the interleaved subcarrier grouping for its superiority, which ensures that the indices of the subcarriers within the β-th group are given by $\Phi_\beta = \{\beta, \beta+g, \ldots, \beta+(n-1)g\}$, where $\beta = 1, \ldots, g$ [26], [37]. The block of incoming bits for the generation of an OFDM symbol is of length m and also split into g blocks, each containing $m/g = p$ bits. For each block, the p bits are further divided into two parts for different purposes. Take the β-th block as a demonstrative example. The first part, comprised of p_1 bits, determines the activation of k out of n subcarriers within the β-th group, whose indices as sorted in ascending order are given by

$$I_\beta = \{i_{\beta,1}, \ldots, i_{\beta,k}\} \tag{1}$$

where $I_\beta \subseteq \Phi_\beta$. The remaining $n-k$ subcarriers are set to be inactive. How to relate a specific SAP to random bits has been solved with a combinatorial method in [24] and will be detailed in Section III.B. Since I_β has $C(n,k)$ possible realizations, we have $p_1 = \lfloor \log_2(C(n,k)) \rfloor$. The second part, comprised of p_2 bits, selects k constellation points independently from the normalized M-ary complex signal set $\mathcal{X}$, yielding

$$\mathbf{s}_\beta = \left[s_\beta(1), \ldots, s_\beta(k) \right]^T \tag{2}$$

where $s_\beta(\gamma) \in \mathcal{X}$ is to be transmitted over the subcarrier of index $i_{\beta,\gamma}$, $\gamma = 1, \ldots, k$. Explicitly, $p_2 = k \log_2(M)$. By taking into account I_β and $\mathbf{s}_\beta$ for all β and concatenating g groups, the frequency-domain OFDM symbol is created as

$$\mathbf{x} = [x(1), \ldots, x(N)]^T \tag{3}$$

where $x(\alpha) \in \{0, \mathcal{X}\}$, $\alpha = 1, \ldots, N$. Before transmission, the inverse fast Fourier transform (FFT) is applied to $\mathbf{x}$ and a cyclic prefix (CP) of length longer than the maximum channel delay spread is appended to the output.

At the receiver, the CP is first removed and the remaining signal is then transformed by the FFT algorithm into the frequency domain, yielding

$$y(\alpha) = h(\alpha) x(\alpha) + w(\alpha), \quad \alpha = 1, \ldots, N \tag{4}$$

where $h(\alpha)$ and $w(\alpha)$ are the channel frequency response (CFR) and the additive white Gaussian noise (AWGN) sample at the α-th subcarrier, respectively. It is assumed that the distributions of $h(\alpha)$ and $w(\alpha)$ are $\mathcal{CN}(0,1)$ and $\mathcal{CN}(0,N_0)$, respectively, where N_0 is the noise variance. From (4) and noting the encoding independence among different groups/blocks, the optimal ML detector for the β-th group can be derived as

$$\left(\hat{I}_\beta, \hat{\mathbf{s}}_\beta\right) = \arg\min_{I_\beta, \mathbf{s}_\beta} \sum_{\lambda=1}^{n} \left| y_\beta(\lambda) \right|^2 + \sum_{\gamma=1}^{k} \left| h\left(i_{\beta,\gamma}\right) s_\beta(\gamma) \right|^2 - 2 \sum_{\gamma=1}^{k} \Re\left\{ y^*\left(i_{\beta,\gamma}\right) h\left(i_{\beta,\gamma}\right) s_\beta(\gamma) \right\}. \tag{5}$$

where $y_\beta(\lambda) = y(\beta + (\lambda-1)g), \beta = 1, \ldots, g$, $\lambda = 1, \ldots, n$. Explicitly, the direct calculation of (5) requires a complexity of order $O(C(n,k)M^k/n)$ per subcarrier, which grows exponentially with M and linearly with $C(n,k)$. For practical use, we can instead resort to the LLR detector [24] or the low-complexity ML detector [25], both enabling single-symbol decoding complexity and near-ML performance. After the detection of the active indices and the modulated symbols, the information bits are recovered by the index demapper and the symbol demodulation.

At this point, we discuss two issues of OFDM-IM related to our work as follows.

[1] *Notation*: Upper and lower case boldface letters denote matrices and vectors, respectively. Superscripts ^{T}, ^{H}, and $^{-1}$ stand for transpose, Hermitian transpose, and inversion operations, respectively. rank$\{\mathbf{X}\}$ and Tr$\{\mathbf{X}\}$ return the rank and the trace of matrix $\mathbf{X}$, respectively. diag$\{\mathbf{x}\}$ creates a diagonal matrix whose diagonal elements are included in $\mathbf{x}$. $\mathbf{I}_n$ denotes the identity matrix of dimensions $n \times n$. $\Re\{\cdot\}$ and $\Im\{\cdot\}$ return the real and imaginary parts of the argument, respectively. $E_X[\cdot]$ represents the expectation over a random variable (RV) X. The probability density function (PDF) and the probability of an event are denoted by $f(\cdot)$ and $\Pr(\cdot)$, respectively. $\mathrm{H}(\cdot)$ and $\mathrm{I}(\cdot,\cdot)$ denote the entropy and the mutual information, respectively. $X \sim \mathcal{CN}(0, \sigma_X^2)$ represents the distribution of a circularly symmetrical complex Gaussian RV X with variance σ_X^2. $\lfloor\cdot\rfloor$, $\lceil\cdot\rceil$, and mod$(\cdot,\cdot)$ denote the floor, ceiling, and modulo operations, respectively. $C(\cdot,\cdot)$ denotes the binomial coefficient. $Q(\cdot)$ denotes the tail probability of the standard Gaussian distribution. $\mathcal{R}$ denotes the set of real numbers. $\langle \mathbf{e}_1, \mathbf{e}_2 \rangle$ denotes the angle between two vectors $\mathbf{e}_1$ and $\mathbf{e}_2$. $\mathbf{e}_1 \cdot \mathbf{e}_2$ denotes the inner product of two vectors $\mathbf{e}_1$ and $\mathbf{e}_2$.

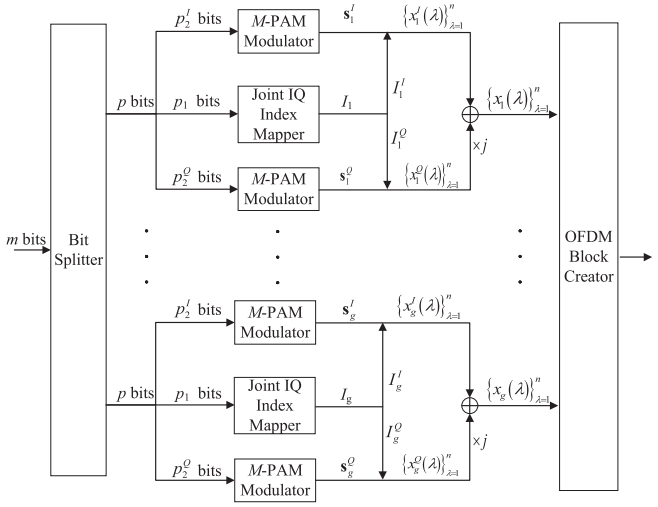

Fig. 2. Block diagram of the OFDM-HIQ-IM transmitter.

1) Spectral Efficiency: Without taking into account the CP, the SE of OFDM-IM systems, measured in bps/Hz, is given by

$$\mathcal{F}_{OFDM-IM} = \frac{p_1 + p_2}{n} = \frac{\lfloor \log_2 (C(n,k)) \rfloor}{n} + \frac{k}{n}\log_2(M) \quad (6)$$

where the first and the second terms at the right hand side are contributed by the IM and the M-ary modulation, respectively. Due to the presence of the exponent k, M^k grows faster than $C(n,k)$ generally, rendering (6) to be limited to the second term in most cases.

2) Diversity Order: Define two diagonal matrices of dimensions $n \times n$, $\mathbf{X}_\beta$ and $\hat{\mathbf{X}}_\beta$, whose diagonal elements represent two different transmission realizations in the frequency domain for the β-th group, given by $[x_\beta(1), \ldots, x_\beta(n)]^T$ and $[\hat{x}_\beta(1), \ldots, \hat{x}_\beta(n)]^T$, respectively, where $x_\beta(\lambda) = x(\beta + (\lambda-1)g), \hat{x}_\beta(\lambda) = \hat{x}(\beta + (\lambda-1)g), \lambda = 1, \ldots, n$. Let $\mathbf{h}_\beta = [h_\beta(1), \ldots, h_\beta(n)]^T$ denote the CFR vector collected from the β-th group, where $h_\beta(\lambda) = h(\beta + (\lambda-1)g), \lambda = 1, \ldots, n$. The diversity order achieved by OFDM-IM systems is shown in [24] to be

$$d_{min} = \min \text{rank}\{\mathbf{K}\mathbf{A}_\beta\} \quad (7)$$

where $\mathbf{K} = E\{\mathbf{h}_\beta \mathbf{h}_\beta^H\}$ is the covariance matrix of $\mathbf{h}_\beta$ and $\mathbf{A}_\beta = (\mathbf{X}_\beta - \hat{\mathbf{X}}_\beta)^H (\mathbf{X}_\beta - \hat{\mathbf{X}}_\beta)$. Noting that $\mathbf{X}_\beta$ is independent of $\hat{\mathbf{X}}_\beta$ with $x_\beta(\lambda), \hat{x}_\beta(\lambda) \in \{0, \mathcal{X}\}$ and $\mathbf{K}$ becomes diagonal for sufficiently large N, we have $d_{min} = 1$, which means the diversity order is limited to unity.

III. The OFDM-HIQ-IM Scheme

To improve the SE of OFDM-IM, we propose OFDM-HIQ-IM in this section.

A. Introduction of OFDM-HIQ-IM

The transmitter structure of OFDM-HIQ-IM is depicted in Fig. 2, where the subsequent inverse FFT and CP insertion operations are removed to highlight the differences from Fig. 1. Similar to OFDM-IM, OFDM-HIQ-IM divides the total OFDM subcarriers into g groups in an interleaved manner and splits the incoming m bits into g blocks, each containing p bits. However, differently, OFDM-HIQ-IM further divides the p bits into three parts rather than two. Let us also focus on the β-th block. The first part, comprised of $p_1 = \lfloor \log_2 (C(n,k^I) C(n,k^Q)) \rfloor$ bits, selects k^I out of n subcarriers to transmit k^I real symbols, and another k^Q out of n subcarriers to transmit k^Q imaginary symbols. The non-selected subcarriers remain idle during communications. The indices of the selected subcarriers are included in $I_\beta = \{I_\beta^I, I_\beta^Q\}$, where

$$I_\beta^I = \{i_{\beta,1}^I, \ldots, i_{\beta,k^I}^I\}, \; I_\beta^Q = \{i_{\beta,1}^Q, \ldots, i_{\beta,k^Q}^Q\} \quad (8)$$

represent the indices of the selected subcarriers that carry the real and imaginary symbols, respectively. The second and the third parts, comprised of $p_2^I = k^I \log_2(M)$ and $p_2^Q = k^Q \log_2(M)$ bits, respectively, generate the k^I real symbols, denoted by $\mathbf{s}_\beta^I = [s_\beta^I(1), \ldots, s_\beta^I(k^I)]^T$, from the normalized M-ary PAM constellation $\mathcal{Z} = \{z_1, \ldots, z_M\}$, and the k^Q imaginary symbols, denoted by $j\mathbf{s}_\beta^Q = j[s_\beta^Q(1), \ldots, s_\beta^Q(k^Q)]^T$, from $j\mathcal{Z}$. Then, by combining the I- and Q- components, the transmitted frequency-domain symbols for the β-th group are generated as $x_\beta(\lambda) = x_\beta^I(\lambda) + j x_\beta^Q(\lambda)$, where $x_\beta^I(\lambda), x_\beta^Q(\lambda) \in \{0, \mathcal{Z}\}, \lambda = 1, \ldots, n$.

After this point, the same procedures as those of OFDM-IM are applied except the ML detection, which can be formulated as (9), shown at the bottom of the next page, where $r(\alpha) \triangleq r^I(\alpha) + j r^Q(\alpha) = y(\alpha)/h(\alpha), \alpha = 1, \ldots, N$, and $r_\beta(\lambda) = r(\beta + (\lambda-1)g), \beta = 1, \ldots, g, \lambda = 1, \ldots, n$. After acquiring $(\hat{I}_\beta, \hat{\mathbf{s}}_\beta^I, \hat{\mathbf{s}}_\beta^Q)$ from (9), which is given at the bottom of the next page, $\hat{I}_\beta$ is de-mapped to the IM bits and $(\hat{\mathbf{s}}_\beta^I, \hat{\mathbf{s}}_\beta^Q)$ are demodulated to obtain the ordinary modulation bits. It is clear from (9) that the ML detector necessitates an exhaustive search through all possible joint I- and Q- SAPs, which incurs a large decoding delay compared with OFDM-IQ-IM. This problem can be significantly alleviated by the proposed low-complexity detectors, as will be introduced in Section III.C.

B. Index Mapping and Demapping

In this subsection, we first describe the implementation of the index mapper and demapper for OFDM-HIQ-IM systems and then clarify the underlying reason for such design.

The mapping of the incoming p_1 bits to I_β involves the following three steps:

1) Step 1: Convert the p_1 bits to an integer $Z \in [0, 2^{p_1} - 1]$;

2) Step 2: Calculate parameters Z^I and Z^Q from

$$Z^I = \left\lfloor \frac{Z}{C(n,k^Q)} \right\rfloor, \quad Z^Q = \text{mod}\left(Z, C(n,k^Q)\right). \quad (10)$$

3) Step 3: Relate I_β^η with Z^η, $\eta \in \{I, Q\}$, according to

$$Z^\eta = C(i_{\beta,k^\eta}^\eta - 1, k^\eta) + \cdots + C(i_{\beta,1}^\eta - 1, 1) \quad (11)$$

TABLE I

ALL POSSIBLE SAPS OF OFDM-IQ-IM AND OFDM-HIQ-IM FOR $n = 4$, $k^I = 2$, AND $k^Q = 2$

OFDM-IQ-IM				OFDM-HIQ-IM							
Z	$\bar{I}_\beta^I, \bar{I}_\beta^Q$	Z	$\bar{I}_\beta^I, \bar{I}_\beta^Q$	Z	$\bar{I}_\beta^I, \bar{I}_\beta^Q$	Z	$\bar{I}_\beta^I, \bar{I}_\beta^Q$	Z	$\bar{I}_\beta^I, \bar{I}_\beta^Q$	Z	$\bar{I}_\beta^I, \bar{I}_\beta^Q$
0	$\{1,2\},\{1,2\}$	8	$\{2,3\},\{1,2\}$	0	$\{1,2\},\{1,2\}$	8	$\{1,3\},\{2,3\}$	16	$\{2,3\},\{2,4\}$	24	$\{2,4\},\{1,2\}$
1	$\{1,2\},\{1,3\}$	9	$\{2,3\},\{1,3\}$	1	$\{1,2\},\{1,3\}$	9	$\{1,3\},\{1,4\}$	17	$\{2,3\},\{3,4\}$	25	$\{2,4\},\{1,3\}$
2	$\{1,2\},\{2,3\}$	10	$\{2,3\},\{2,3\}$	2	$\{1,2\},\{2,3\}$	10	$\{1,3\},\{2,4\}$	18	$\{1,4\},\{1,2\}$	26	$\{2,4\},\{2,3\}$
3	$\{1,2\},\{1,4\}$	11	$\{2,3\},\{1,4\}$	3	$\{1,2\},\{1,4\}$	11	$\{1,3\},\{3,4\}$	19	$\{1,4\},\{1,3\}$	27	$\{2,4\},\{1,4\}$
4	$\{1,3\},\{1,2\}$	12	$\{1,4\},\{1,2\}$	4	$\{1,2\},\{2,4\}$	12	$\{2,3\},\{1,2\}$	20	$\{1,4\},\{2,3\}$	28	$\{2,4\},\{2,4\}$
5	$\{1,3\},\{1,3\}$	13	$\{1,4\},\{1,3\}$	5	$\{1,2\},\{3,4\}$	13	$\{2,3\},\{1,3\}$	21	$\{1,4\},\{1,4\}$	29	$\{2,4\},\{3,4\}$
6	$\{1,3\},\{2,3\}$	14	$\{1,4\},\{2,3\}$	6	$\{1,3\},\{1,2\}$	14	$\{2,3\},\{2,3\}$	22	$\{1,4\},\{2,4\}$	30	$\{3,4\},\{1,2\}$
7	$\{1,3\},\{1,4\}$	15	$\{1,4\},\{1,4\}$	7	$\{1,3\},\{1,3\}$	15	$\{2,3\},\{1,4\}$	23	$\{1,4\},\{3,4\}$	31	$\{3,4\},\{1,3\}$

where i^η_{β,k^η} is the maximal integer that satisfies $Z^\eta \geq C(i^\eta_{\beta,k^\eta}-1,k^\eta)$, and $i^\eta_{\beta,k^\eta-1}$ is the maximal integer that satisfies $Z^\eta - C(i^\eta_{\beta,k^\eta}-1,k^\eta) \geq C(i^\eta_{\beta,k^\eta-1}-1,k^\eta-1)$, and so on. Note that this step is exactly the so-called combinatorial method in [24].

The mapping of I_β to p_1 bits follows a reverse process. Specifically, we first obtain Z^I and Z^Q from (11), and then calculate Z from $Z = Z^I C(n,k^Q) + Z^Q$, and finally convert Z from decimal to binary.

From above, an example of $(n,k^I,k^Q) = (4,2,2)$ is presented in Table I, where $\bar{I}^\eta_\beta = (I^\eta_\beta - \beta)/g + 1$, $\eta \in \{I,Q\}$, and all possible SAPs of OFDM-HIQ-IM are listed. For comparison, we also list the SAP set selected by OFDM-IQ-IM. It should be noted that though OFDM-HIQ-IM explores both I- and Q- dimensions, it involves more active elements than OFDM-IQ-IM for IM. In OFDM-IQ-IM, I^I_β and I^Q_β are independently selected by the IM bits, which, as a result, can only encode $2^{\lfloor \log_2(C(n,k^I))\rfloor + \lfloor \log_2(C(n,k^Q))\rfloor}$ active elements [25], [31]. However, in OFDM-HIQ-IM, I^I_β and I^Q_β are jointly selected, which allows encoding of $2^{\lfloor \log_2(C(n,k^I)C(n,k^Q))\rfloor}$ active elements. Therefore, in this example, we see that there are in total 16 SAPs for OFDM-IQ-IM, while this number is doubled for OFDM-HIQ-IM, which means one more IM bit per group can be conveyed by OFDM-HIQ-IM.

Clearly, the SE of the OFDM-HIQ-IM system is given by

$$\mathcal{F}_{HIQ} = \frac{1}{n}\left\lfloor \log_2\left(C\left(n,k^I\right)C\left(n,k^Q\right)\right)\right\rfloor + \frac{k^I+k^Q}{n}\log_2(M). \quad (12)$$

If we let $k^I = k^Q = k$ and all symbols carried on the I- and Q- branches be $\sqrt{M}$-PAM modulated in (12), the SE of OFDM-HIQ-IM becomes (6) except that $C(n,k)$ is replaced with $C^2(n,k)$, which implies that a considerably improved SE is achieved compared with OFDM-IM.

Remark: It should be noted that OFDM-HIQ-IM does not fully explore the I- and Q- dimensions since it requires a fixed number of active subcarriers on each dimension. In fact, much more possible SAPs, which have a total number of $2^{\lfloor \log_2(C(2n,k^I+k^Q))\rfloor}$, can be exploited to transmit the same number of k^I+k^Q symbols without this constraint. However, despite a significant expansion of the index domain in this manner, a large portion of SAPs would become difficult to differentiate due to their lower inter-SAP Euclidean distances, which in turn deteriorates the BER performance. This can be understood via the following example. Assume $(n,k^I+k^Q) = (4,4)$ and two SAPs $\{\bar{I}^I_{\beta_1},\bar{I}^Q_{\beta_1}\} = \{\{1,2,3,4\},\{\}\}$ and $\{\bar{I}^I_{\beta_2},\bar{I}^Q_{\beta_2}\} = \{\{2,3,4\},\{1\}\}$. Then, it can be shown that the pairwise error probability (PEP) between these two SAPs, namely $\Pr\left(\{\bar{I}^I_{\beta_1},\bar{I}^Q_{\beta_1}\} \to \{\bar{I}^I_{\beta_2},\bar{I}^Q_{\beta_2}\}\right)$, will be much higher than that between any two SAPs of OFDM-HIQ-IM in Table I at high SNR since the former declines with the first power of SNR while the latter decreases with at least the square of SNR. Therefore, considering that OFDM-HIQ-IM successfully avoids the problem of diversity loss for the PEP events involving different SAPs while achieving SE improvement, it is much preferred. Another reason for this preference is that OFDM-HIQ-IM enables low-complexity detection, as will be shown in the next subsection.

C. Low-Complexity Detectors

The ML detection in (9) is optimal; however, it leads to a prohibitive computational complexity, which is of order $O(2^{p_1}M(k^I+k^Q)/n)$ per subcarrier. To solve this problem, we propose two sub-optimal detection methods with significantly reduced computational complexity, called LLR detector and low-complexity ML detector, for OFDM-HIQ-IM in this subsection.

1) LLR Detector: For LLR detection, the first step is to calculate the LLR values associated with the $2n$ I- and Q- components for each group, which are defined as the ratio between the probabilities of activation and inactivation [24]:

$$L^\eta_\beta(\lambda) \propto \frac{\left|h_\beta(\lambda)\, r^\eta_\beta(\lambda)\right|^2}{N_0/2} + \ln\left(\sum_{\epsilon=1}^{M} e^{-\frac{|h_\beta(\lambda)|^2}{N_0/2}\left(r^\eta_\beta(\lambda)-z_\epsilon\right)^2}\right), \quad \eta \in \{I,Q\} \quad (13)$$

$$\left(\hat{I}_\beta, \hat{\mathbf{s}}^I_\beta, \hat{\mathbf{s}}^Q_\beta\right) = \underset{I_\beta,\mathbf{s}^I_\beta,\mathbf{s}^Q_\beta}{\arg\min} \sum_{\kappa=1}^{k^I} |h\left(i^I_{\beta,\kappa}\right)|^2 [s^I_\beta(\kappa)\left(s^I_\beta(\kappa) - 2r^I\left(i^I_{\beta,\kappa}\right)\right)] + \sum_{\nu=1}^{k^Q} |h(i^Q_{\beta,\nu})|^2 [s^Q_\beta(\nu)\,(s^Q_\beta(\nu) - 2r^Q(i^Q_{\beta,\nu}))] \quad (9)$$

TABLE II
COMPLEXITY COMPARISON BETWEEN LLR, LOW-COMPLEXITY ML, AND ML DETECTORS

$(n, k^I, k^Q), M$	LLR Detector	Low-Complexity ML Detector	ML Detector
$(4,2,2),2$	4	4	64
$(4,2,3),2$	4	4	40
$(8,5,6),4$	8	8	5632
$(8,6,6),4$	8	8	3072

where $\beta = 1, \ldots, g$. The second step is to sort $[L_\beta^\eta(1), \ldots, L_\beta^\eta(n)]^T$ in descending order and pick out the first k^η ones, whose corresponding subcarriers of indices $\hat{I}_\beta^\eta = \{\hat{i}_{\beta,1}^\eta, \ldots, \hat{i}_{\beta,k^\eta}^\eta\}$ are regarded to be active, where $\eta \in \{I, Q\}$. The third step is to search for the most likely modulated symbol carried on the active subcarriers via

$$\hat{s}_\beta^\eta(\tau) = \arg\min_{s_\beta^\eta(\tau)} \left(r_\beta^\eta\left(\hat{i}_{\beta,\tau}^\eta\right) - s_\beta^\eta(\tau)\right)^2, \quad \tau = 1, \ldots, k^\eta, \eta \in \{I, Q\}. \tag{14}$$

Finally, $\hat{I}_\beta$ is de-mapped to the IM bits according to the method described in Section III.A and $(\hat{\mathbf{s}}_\beta^I, \hat{\mathbf{s}}_\beta^Q)$ are demodulated to obtain the ordinary modulation bits. From above, it is clear that the computational complexity of the LLR detector is only of order $O(2M)$ per subcarrier.

2) Low-Complexity ML Detector: The idea of the low-complexity ML detector is to decouple the detection of the in-phase and quadrature components from (9). It is comprised of four steps. The first step is to search for the most likely modulated symbols carried on all subcarriers within a group assuming they are all active:

$$\tilde{s}_\beta^\eta(\alpha) = \arg\min_{s \in \mathcal{Z}} \left(r_\beta^\eta(\alpha) - s\right)^2, \quad \eta \in \{I, Q\} \tag{15}$$

where $\beta = 1, \ldots, g$ and $\alpha = 1, \ldots, n$. Due to IM, the desired outputs are not all but k^η elements of $\tilde{\mathbf{s}}_\beta^\eta = [\tilde{s}_\beta^\eta(1), \ldots, \tilde{s}_\beta^\eta(n)]^T$, whose locations are to be determined. The second step is to calculate the so-called ML decision metrics associated with $2n$ I- and Q- components for per group via

$$M_\beta^\eta(\alpha) = |h_\beta(\alpha)|^2 \left[\tilde{s}_\beta^\eta(\alpha)\left(\tilde{s}_\beta^\eta(\alpha) - 2r_\beta^\eta(\alpha)\right)\right], \quad \eta \in \{I, Q\} \tag{16}$$

where $\beta = 1, \ldots, g$ and $\alpha = 1, \ldots, n$. The third step is to first sort $[M_\beta^\eta(1), \ldots, M_\beta^\eta(n)]^T$ in ascending order and pick out the first k^η ones, whose corresponding subcarriers of indices $\hat{I}_\beta^\eta = \{\hat{i}_{\beta,1}^\eta, \ldots, \hat{i}_{\beta,k^\eta}^\eta\}$ are regarded to be active, and then obtain the desired modulated symbols from

$$\hat{s}_\beta^I(\kappa) = \tilde{s}_\beta^I\left(i_{\beta,\kappa}^I\right), \quad \hat{s}_\beta^Q(\nu) = \tilde{s}_\beta^Q\left(i_{\beta,\nu}^Q\right), \quad \kappa = 1, \ldots, k^I, \quad \nu = 1, \ldots, k^Q \tag{17}$$

where $\eta \in \{I, Q\}$. The final step is to recover the information bits from $(\hat{I}_\beta, \hat{\mathbf{s}}_\beta^I, \hat{\mathbf{s}}_\beta^Q)$, which is the same as that of the LLR detector. Compared to the LLR detector, one can see that the low-complexity ML detector has nearly the same computational complexity, namely of order $O(2M)$ per subcarrier. This can be understood since both detectors resort to decoupled detection and calculate the LLR/ML decision metrics for all subcarriers.

3) Complexity Comparison: To compare the computational complexity of the two proposed sub-optimal detectors, namely the LLR and low-complexity ML detectors, with that of the ML detector, we consider the average number of metric calculations per subcarrier as a performance metric, whose values associated with the above three detectors, as discussed earlier, can be calculated by $2M$, $2M$, and $2^{p_1}M(k^I + k^Q)/n$, respectively. Table II presents the comparison results for some given system parameters. As seen from Table II, while the computational complexity of the ML detector is highly susceptible to parameters n, k^I, k^Q, and M, that of the two proposed detectors is only determined by M and, apparently, much lower than the former.

D. Performance Analysis

In this subsection, we derive an asymptotically tight upper bound on the BER of the OFDM-HIQ-IM system using ML detection and analyze its achievable rate. Since the encoding and decoding processes for each group are the same and independent, without loss of generality we only focus on the β-th group.

1) BER Upper Bound: For ease of analysis, we assume the independence between the I- and Q- branches such that the errors on both branches can be analyzed separately. Note that this assumption becomes true when $C(n, k^I)C(n, k^Q)$ is an integer power of two.[2] For brevity, we only derive the error on the in-phase branch. The probability of the event that $\mathbf{X}_\beta^I$ is transmitted but erroneously detected as $\hat{\mathbf{X}}_\beta^I$ conditioned on $\mathbf{h}_\beta$ can be expressed from (9) as

$$\Pr\left(\mathbf{X}_\beta^I \to \hat{\mathbf{X}}_\beta^I \middle| \mathbf{h}_\beta\right) = Q\left(\sqrt{\frac{1}{2N_0}\left\|\left(\mathbf{X}_\beta^I - \hat{\mathbf{X}}_\beta^I\right)\mathbf{h}_\beta\right\|^2}\right). \tag{18}$$

Then, according to the identity $Q(x) \approx \frac{1}{12}e^{-x^2/2} + \frac{1}{4}e^{-2x^2/3}$, the unconditioned PEP can be readily derived from (18) as [24]

$$\Pr\left(\mathbf{X}_\beta^I \to \hat{\mathbf{X}}_\beta^I\right) = E_{\mathbf{h}_\beta}\left\{\Pr\left(\mathbf{X}_\beta^I \to \hat{\mathbf{X}}_\beta^I \middle| \mathbf{h}_\beta\right)\right\} = \frac{1/12}{\det\left(\mathbf{I}_n + q_1\mathbf{K}\mathbf{A}_\beta^I\right)} + \frac{1/4}{\det\left(\mathbf{I}_n + q_2\mathbf{K}\mathbf{A}_\beta^I\right)} \tag{19}$$

[2]Of course, we can incorporate the dependence between the I- and Q- branches, which is true for OFDM-HIQ-IM, into the analysis. In this case, we have to average $\Pr(\mathbf{X}_\beta \to \hat{\mathbf{X}}_\beta)$ over all possible $\mathbf{X}_\beta$ and $\hat{\mathbf{X}}_\beta$. However, the decision zones overlap much more than those by averaging $\Pr(\mathbf{X}_\beta^I \to \hat{\mathbf{X}}_\beta^I)$ over all possible $\mathbf{X}_\beta^I$ and $\hat{\mathbf{X}}_\beta^I$, leading to a looser upper bound. The tightness of the proposed upper bound under the independence assumption will be validated in Section V.

where $\mathbf{A}_\beta^I = (\mathbf{X}_\beta^I - \hat{\mathbf{X}}_\beta^I)^H(\mathbf{X}_\beta^I - \hat{\mathbf{X}}_\beta^I)$, $q_1 = 1/(2N_0)$, and $q_2 = 2/(3N_0)$. In the same manner, the probability of the event that $\mathbf{X}_\beta^Q$ is transmitted but erroneously detected as $\hat{\mathbf{X}}_\beta^Q$ is given by

$$\Pr\left(\mathbf{X}_\beta^Q \to \hat{\mathbf{X}}_\beta^Q\right) = \frac{1/12}{\det\left(\mathbf{I}_n + q_1\mathbf{K}\mathbf{A}_\beta^Q\right)} + \frac{1/4}{\det\left(\mathbf{I}_n + q_2\mathbf{K}\mathbf{A}_\beta^Q\right)} \tag{20}$$

where $\mathbf{A}_\beta^Q = (\mathbf{X}_\beta^Q - \hat{\mathbf{X}}_\beta^Q)^H(\mathbf{X}_\beta^Q - \hat{\mathbf{X}}_\beta^Q)$. Finally, the BER of OFDM-HIQ-IM can be upper bounded according to the union bounding technique by

$$P_e \le \frac{1}{p2^p}\sum_{\mathbf{X}_\beta}\sum_{\hat{\mathbf{X}}_\beta}\Pr\left(\mathbf{X}_\beta^I \to \hat{\mathbf{X}}_\beta^I\right) \times \Pr\left(\mathbf{X}_\beta^Q \to \hat{\mathbf{X}}_\beta^Q\right) e\left(\mathbf{X}_\beta, \hat{\mathbf{X}}_\beta\right) \tag{21}$$

where $e(\mathbf{X}_\beta, \hat{\mathbf{X}}_\beta)$ represents the number of bits in difference between $\mathbf{X}_\beta$ and $\hat{\mathbf{X}}_\beta$. From (20), it is easy to verify that the diversity order achieved by the OFDM-HIQ-IM system is also given by (7), which turns out to be unity.

2) Achievable Rate: Conditioned on the channel, the channel output $\mathbf{y}_\beta = \left[y_\beta(1), \ldots, y_\beta(n)\right]^T$ has the multivariate PDFs of

$$f\left(\mathbf{y}_\beta|\mathbf{X}_\beta, \mathbf{h}_\beta\right) = \frac{1}{(\pi N_0)^n} e^{-\frac{1}{N_0}\|\mathbf{y}_\beta - \mathbf{X}_\beta\mathbf{h}_\beta\|^2} \tag{22}$$

$$f\left(\mathbf{y}_\beta|\mathbf{h}_\beta\right) = E_{\mathbf{X}_\beta}\left\{f\left(\mathbf{y}_\beta|\mathbf{X}_\beta, \mathbf{h}_\beta\right)\right\} = \frac{1}{2^p}\sum_{\vartheta=1}^{2^p} f\left(\mathbf{y}_\beta|\mathbf{X}_\beta^{(\vartheta)}, \mathbf{h}_\beta\right) \tag{23}$$

where $\mathbf{X}_\beta^{(\vartheta)}$ is the ϑ-th realization of $\mathbf{X}_\beta$, $\vartheta = 1, \ldots, 2^p$. The achievable rate of OFDM-HIQ-IM systems is defined as the mutual information between the channel input $\mathbf{X}_\beta$ and the channel output $\mathbf{y}_\beta$ averaged over the subcarriers [26], which can be calculated from (22) and (23) by (24) (bps/Hz), shown at the top of the next page, where $\mathcal{F}_{HIQ}$ is given by (12) and $\mathbf{w}_\beta = [w(\beta), \ldots, w(\beta + (n-1)g)]^T$. To our best knowledge, no closed form solution is available for (24). However, in analogy with [26], (24) can be approximated in a simple form by

$$\mathcal{R}_{HIQ} \approx \mathcal{F}_{HIQ} - \frac{1}{2^p n}\sum_{\varpi=1}^{2^p}\log_2\left(\sum_{\vartheta=1}^{2^p}\frac{1}{\det\left(\mathbf{I}_n + \mathbf{K}\mathbf{U}_{\varpi,\vartheta}\right)}\right) \tag{25}$$

where $\mathbf{U}_{\varpi,\vartheta} = \frac{1}{2N_0}(\mathbf{X}_\beta^{(\varpi)} - \mathbf{X}_\beta^{(\vartheta)})^H(\mathbf{X}_\beta^{(\varpi)} - \mathbf{X}_\beta^{(\vartheta)})$. This approximation is derived by applying Jensen's inequality and adding $1/\ln(2) - 1$, which is accurate in both low and high SNR regions.

IV. The LP-OFDM-IQ-IM Scheme

As indicated in Section III, the diversity order of OFDM-IM systems depends on the minimum of $(\text{rank}\{\mathbf{K}\}, \text{rank}\{\mathbf{A}_\beta\})$, where $\mathbf{K}$ and $\mathbf{A}_\beta$ are defined in (7). With interleaved grouping, all subcarriers within a group probably experience independent fading; therefore, $\mathbf{K}$ has full rank and the diversity order is only determined by $\text{rank}\{\mathbf{A}_\beta\}$.

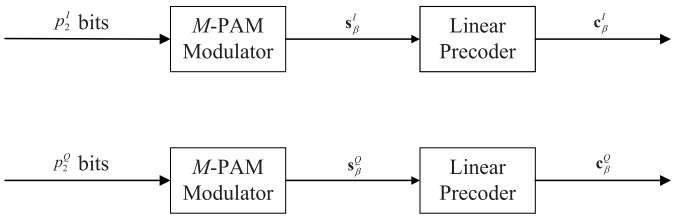

Fig. 3. The main operation of the LP-OFDM-IQ-IM transmitter.

Recalling that $\mathbf{A}_\beta = (\mathbf{X}_\beta - \hat{\mathbf{X}}_\beta)^H(\mathbf{X}_\beta - \hat{\mathbf{X}}_\beta)$, it can be found that if the IM bits associated with $\mathbf{X}_\beta$ and $\hat{\mathbf{X}}_\beta$ are different, namely $\mathbf{X}_\beta$ and $\hat{\mathbf{X}}_\beta$ have different SAPs, we always have $\text{rank}\{\mathbf{A}_\beta\} \ge 2$; otherwise, it follows that $\text{rank}\{\mathbf{A}_\beta\} \ge 1$, where the equality holds when $\mathbf{X}_\beta$ and $\hat{\mathbf{X}}_\beta$ have only one different diagonal element, namely the error only occurs on the modulated symbol carried on a subcarrier. In a nutshell, the IM bits have two-diversity-order protection while the ordinary modulation bits have only one-diversity-order protection (see Remarks 1 and 3 of [24]). Please note that this property in not valid for plain SM-based systems since they employ only transmit antenna indices of a MIMO system for IM purposes. On the other hand, this property in fact applies to many other index modulated OFDM systems besides OFDM-IM, such as OFDM-IQ-IM and OFDM-HIQ-IM. Motivated by the above finding, we aim at improving the diversity order achieved by the ordinary modulation bits from unity to two while maximizing the overall coding gain. To this end, we resort to the idea of the well-known LCP technique. To obtain a larger SE, we assume that the IM operates on both I- and Q- branches, thus applying to the OFDM-IQ-IM and OFDM-HIQ-IM systems. Due to its nature, the proposed scheme can be called as LP-OFDM-IQ-IM. In this section, we first introduce the principle of LP-OFDM-IQ-IM and then derive the optimal precoding matrices.

A. Principle of LP-OFDM-IQ-IM

The transmitter structure of LP-OFDM-IQ-IM is the same as that of OFDM-HIQ-IM in Fig. 2 (or OFDM-IQ-IM) except that an additional linear precoder is employed following the M-PAM modulator. For comparison convenience, we highlight the differences in Fig. 3. Since the encoding and decoding processes of the I- and Q- branches are similar, we only focus on the in-phase branch in the following for brevity. Considering the β-th group, the p_2^I bits pass through the M-ary modulator, generating $\mathbf{s}_\beta^I = \left[s_\beta^I(1), \ldots, s_\beta^I\left(k^I\right)\right]^T$. Then, $\mathbf{s}_\beta^I$ is divided into $k^I/2$ pairs, each precoded by

$$\mathbf{B} = \begin{bmatrix} b_{11} & b_{12} \\ b_{21} & b_{22} \end{bmatrix} \tag{26}$$

where the elements are drawn from $\mathcal{R}$ and the constraint, $b_{i1}^2 + b_{i2}^2 = 1, i = 1, 2$, is imposed to guarantee the same power as the input. Therefore, the output of the linear precoder

$$\begin{aligned}\mathcal{R}_{HIQ} &= \frac{\mathrm{I}\left(\mathbf{X}_\beta, \mathbf{y}_\beta\right)}{n} = \frac{\mathrm{H}\left(\mathbf{X}_\beta\right)}{n} + \frac{\mathrm{H}\left(\mathbf{X}_\beta|\mathbf{y}_\beta\right)}{n} \\ &= \mathcal{F}_{HIQ} - \frac{1}{n2^p}\sum_{\varpi=1}^{2^p} E_{\mathbf{h}_\beta}\left\{\int f\left(\mathbf{y}_\beta|\mathbf{X}_\beta^{(\varpi)}, \mathbf{h}_\beta\right)\log_2\left(\frac{f\left(\mathbf{X}_\beta^{(\varpi)}, \mathbf{y}_\beta|, \mathbf{h}_\beta\right)}{f\left(\mathbf{y}_\beta|\mathbf{h}_\beta\right)}\right)d\mathbf{y}_\beta\right\} \\ &= \mathcal{F}_{HIQ} - \left(\frac{1}{\ln 2} - 1\right) - \frac{1}{n2^p}\sum_{\varpi=1}^{2^p} E_{\mathbf{h}_\beta,\mathbf{w}_\beta}\left\{\sum_{\vartheta=1}^{2^p}\log_2\left(2^n e^{-\frac{1}{N_0}\left\|\mathbf{w}_\beta + \left(\mathbf{X}_\beta^{(\varpi)} - \mathbf{X}_\beta^{(\vartheta)}\right)\mathbf{h}_\beta\right\|^2}\right)\right\} \end{aligned} \tag{24}$$

is given by

$$\mathbf{c}_\beta^I = \begin{bmatrix} c_\beta^I(1) \\ c_\beta^I(2) \\ \vdots \\ c_\beta^I\left(k^I-1\right) \\ c_\beta^I\left(k^I\right)\end{bmatrix} = \begin{bmatrix} \mathbf{B}\begin{bmatrix} s_\beta^I(1) \\ s_\beta^I(2)\end{bmatrix} \\ \vdots \\ \mathbf{B}\begin{bmatrix} s_\beta^I\left(k^I-1\right) \\ s_\beta^I\left(k^I\right)\end{bmatrix}\end{bmatrix} = \begin{bmatrix} b_{11}s_\beta^I(1) + b_{12}s_\beta^I(2) \\ b_{21}s_\beta^I(1) + b_{22}s_\beta^I(2) \\ \vdots \\ b_{11}s_\beta^I\left(k^I-1\right) + b_{12}s_\beta^I\left(k^I\right) \\ b_{21}s_\beta^I\left(k^I-1\right) + b_{22}s_\beta^I\left(k^I\right)\end{bmatrix}. \tag{27}$$

Finally, $\mathbf{c}_\beta^I$ is transmitted over the k^I active subcarriers of indices I_β^I, which are determined by the IM bits, such that $c_\beta^I(\kappa) = x^I\left(i_{\beta,\kappa}^I\right)$, $\kappa = 1, \ldots, k^I$.

The received signal in the frequency domain can be expressed in the same form as (4), for which the optimal ML detection for the in-phase branch can be formulated as (28), shown at the top of the next page, where $c_\beta^I(2\xi-1) = b_{11}s_\beta^I(2\xi-1) + b_{12}s_\beta^I(2\xi)$ and $c_\beta^I(2\xi) = b_{21}s_\beta^I(2\xi-1) + b_{22}s_\beta^I(2\xi)$. Since the elements of $\mathbf{s}_\beta^I$ are independent of each other, for a given I_β^I, we can search for them pair by pair from (28). Consequently, the computational complexity of (28) is on the order of $\mathcal{O}\left(C\left(n, k^I\right)M^2k^I/2n\right)$ per subcarrier, which can be prohibitive for large n and k^I.

Similar to the case of OFDM-HIQ-IM, the computational complexity can be significantly reduced by employing the LLR detector that has near-ML performance. To show this, let $\mathcal{U}_1 = \{b_{11}s_1 + b_{12}s_2, \forall s_1, s_2 \in \mathcal{Z}\}$ and $\mathcal{U}_2 = \{b_{21}s_1 + b_{22}s_2, \forall s_1, s_2 \in \mathcal{Z}\}$. First, the LLR detector calculates the LLR values associated with all subcarriers within a group by

$$L_\beta^I(\lambda) \propto \ln\left(\sum_{u\in\mathcal{U}_1\cup\mathcal{U}_2} e^{-\frac{|h_\beta(\lambda)|^2}{N_0}\left(r_\beta^I(\lambda)-u\right)^2}\right) + \frac{\left|h_\beta(\lambda)\, r_\beta^I(\lambda)\right|^2}{N_0}, \quad \lambda = 1, \ldots, n. \tag{29}$$

Then, it decides upon k^I active indices out of them having the maximum values. Once the active indices $\hat{I}_\beta^I$ are determined, the modulated symbols are estimated pair by pair as (30), shown at the top of the next page, where $\xi = 1, \ldots, k^I/2$. Since (29) and (30) involve $2nM^2$ and $M^2k^I/2$ searches, the computational complexity of the LLR detector is on the order of $\mathcal{O}(M^2(2 + k^I/2n))$ per subcarrier.

B. Optimal Design

Following the methodology in Section III.D, the BER of LP-OFDM-IQ-IM can be upper bounded in the same form as (21), whose value highly depends on the choice of the precoding matrix $\mathbf{B}$. In this subsection, we focus on the design of $\mathbf{B}$ aiming at optimizing the asymptotic BER performance. For brevity, we only take the in-phase branch for demonstration.

At high SNR, the PEP approximates to [24]

$$\Pr\left(\mathbf{X}_\beta^I \to \hat{\mathbf{X}}_\beta^I\right) \approx \left(\prod_{\omega=1}^{d}\delta_\omega\left(\mathbf{K}\mathbf{A}_\beta^I\right)\right)^{-1} \times \left(\frac{4^d}{12} + \frac{3^d}{4}\right)\left(\frac{N_0}{2}\right)^d \tag{31}$$

where $d = \mathrm{rank}\left\{\mathbf{K}\mathbf{A}_\beta^I\right\}$ and $\delta_\omega\left(\mathbf{K}\mathbf{A}_\beta^I\right)$, $\omega = 1, \ldots, d$, are the nonzero eigenvalues of $\mathbf{K}\mathbf{A}_\beta^I$. Assuming that the subcarriers within a group are faded independently, which can be ensured in practice by interleaved grouping [26], we obtain $\mathbf{K} = \mathbf{I}_n$. Therefore, the optimization problem can be formulated by maximizing the minimum coding gain distance (CGD) as[3]

$$\begin{aligned}\mathbf{B}_{opt} = \arg\max_{\mathbf{B}}\left\{\min_{\mathbf{X}_\beta^I, \hat{\mathbf{X}}_\beta^I}\delta_1\left(\mathbf{A}_\beta^I\right)\delta_2\left(\mathbf{A}_\beta^I\right)\right\} \\ s.t.\ b_{i1}^2 + b_{i2}^2 = 1, \quad i = 1, 2.\end{aligned} \tag{32}$$

Through carefully examining $\mathbf{A}_\beta^I$, we find that there are only two different situations that satisfy $\mathrm{rank}\{\mathbf{A}_\beta^I\} = 2$. The first situation is that $\mathbf{X}_\beta^I$ and $\hat{\mathbf{X}}_\beta^I$ have the same SAP and only a pair of modulated symbols associated with them for precoding, denoted by (s_1, s_2) and $(\hat{s}_1, \hat{s}_2)$, are different, where $s_i, \hat{s}_i \in \mathcal{Z}, i = 1, 2$, and $(s_1, s_2) \neq (\hat{s}_1, \hat{s}_2)$. In this situation, it can be readily figured out (33), shown at the top of the next page, where $\Delta s_i = s_i - \hat{s}_i, i = 1, 2$. The other situation is that there are no erroneous modulated symbols,

[3]It should be noted that with the goal of maximizing the overall coding gain, the optimization problem should be formulated as $\arg\max\sum_{\mathbf{X}_\beta^I, \hat{\mathbf{X}}_\beta^I}\delta_1\left(\mathbf{A}_\beta^I\right)\delta_2\left(\mathbf{A}_\beta^I\right)e\left(\mathbf{X}_\beta^I, \hat{\mathbf{X}}_\beta^I\right)$, *s.t.* $d = 2$ rather than (32). However, this invokes the joint design of the bit encoding scheme and the precoding matrix, which is quite complicated. To circumvent this problem, we resort to the well-known max-min method in (32), which only considers the effect of PEP regardless of the number of bits in error due to its dominance. It will be shown that the max-min method significantly simplifies the analysis and more importantly enables closed-form solutions.

$$\left(\hat{I}_\beta^I, \hat{\mathbf{s}}_\beta^I\right) = \underset{I_\beta^I, \mathbf{s}_\beta^I}{\arg\min} \sum_{\lambda=1}^{n} \left|h_\beta(\lambda)\right|^2 \left[r_\beta^I(\lambda) - x_\beta^I(\lambda)\right]^2 = \underset{I_\beta^I, \mathbf{s}_\beta^I}{\arg\min} \sum_{\kappa=1}^{k^I} \left|h\left(i_{\beta,\kappa}^I\right)\right|^2 c_\beta^I(\kappa) \left[c_\beta^I(\kappa) - 2r^I\left(i_{\beta,\kappa}^I\right)\right]$$
$$= \underset{I_\beta^I, \mathbf{s}_\beta^I}{\arg\min} \sum_{\xi=1}^{k^I/2} \left\{ \begin{array}{l} \left|h\left(i_{\beta,2\xi-1}^I\right)\right|^2 c_\beta^I(2\xi-1) \left[c_\beta^I(2\xi-1) - 2r^I\left(i_{\beta,2\xi-1}^I\right)\right] \\ +\left|h\left(i_{\beta,2\xi}^I\right)\right|^2 c_\beta^I(2\xi) \left[c_\beta^I(2\xi) - 2r^I\left(i_{\beta,2\xi}^I\right)\right] \end{array} \right\} \tag{28}$$

$$\left(\hat{s}_\beta^I(2\xi-1), \hat{s}_\beta^I(2\xi)\right) = \underset{s_\beta^I(2\xi-1), s_\beta^I(2\xi)}{\arg\min} \left\{ \begin{array}{l} \left|h\left(\hat{i}_{\beta,2\xi-1}^I\right)\right|^2 \left[r^I\left(\hat{i}_{\beta,2\xi-1}^I\right) - c_\beta^I(2\xi-1)\right]^2 \\ +\left|h\left(\hat{i}_{\beta,2\xi}^I\right)\right|^2 \left[r^I\left(\hat{i}_{\beta,2\xi}^I\right) - c_\beta^I(2\xi)\right]^2 \end{array} \right\} \tag{30}$$

$$\delta_1\left(\mathbf{A}_\beta^I\right)\delta_2\left(\mathbf{A}_\beta^I\right) = \begin{cases} \left|(\Delta s_1)^2 b_{11} b_{21}\right|^2, & \text{for } \Delta s_1 \neq 0,\ \Delta s_2 = 0 \\ \left|(\Delta s_2)^2 b_{12} b_{22}\right|^2, & \text{for } \Delta s_1 = 0,\ \Delta s_2 \neq 0 \\ \left|(\Delta s_1 b_{11} + \Delta s_2 b_{12})(\Delta s_1 b_{21} + \Delta s_2 b_{22})\right|^2, & \text{for } \Delta s_1 \neq 0,\ \Delta s_2 \neq 0 \end{cases} \tag{33}$$

$$\mathbf{B}_{opt} = \underset{\mathbf{B}}{\arg\max} \left\{ \min \left\{ \begin{array}{l} \left|(\Delta s_1)^2 b_{11} b_{21}\right|, \left|(\Delta s_2)^2 b_{12} b_{22}\right|, \\ \left|(\Delta s_1 b_{11} + \Delta s_2 b_{12})(\Delta s_1 b_{21} + \Delta s_2 b_{22})\right|, \\ (s_1 b_{11} + s_2 b_{12})^2, (s_1 b_{21} + s_2 b_{22})^2 \end{array} \right\} \right\} \quad s.t.\ b_{i1}^2 + b_{i2}^2 = 1, \quad i = 1, 2. \tag{34}$$

$$g_2^2(t_2, t_1) - g_1^2(t_1, t_2) = (t_1 \sin\theta + t_2 \cos\theta)^2 \left[(t_1 \sin\theta + t_2 \cos\theta)^2 - (t_1 \cos\theta + t_2 \sin\theta)^2\right] \leq 0. \tag{35}$$

i.e., $(s_1, s_2) = (\hat{s}_1, \hat{s}_2)$, and there is only one different active index between $\mathbf{X}_\beta^I$ and $\hat{\mathbf{X}}_\beta^I$. In this situation, corresponding to the difference lying at the first or second active index, respectively, it can be readily figured out that $\delta_1(\mathbf{A}_\beta^I)\delta_2(\mathbf{A}_\beta^I) = (s_1 b_{11} + s_2 b_{21})^4$ or $\delta_1(\mathbf{A}_\beta^I)\delta_2(\mathbf{A}_\beta^I) = (s_1 b_{21} + s_2 b_{22})^4$. Therefore, (32) can be further simplified as (34), shown at the top of this page.

Lemma 1: If $\left[b_{11}^*, b_{12}^*; b_{21}^*, b_{22}^*\right]$ is a solution to (34), $\left[\pm\left|b_{11}^*\right|, \pm\left|b_{12}^*\right|; \pm\left|b_{21}^*\right|, \pm\left|b_{22}^*\right|\right]$ is also a solution.

Proof: We will only prove that $\left[b_{11}^*, -b_{12}^*; -b_{21}^*, b_{22}^*\right]$ is also a solution to (34) since the proof for the other forms can be performed in a similar manner.

From (34), the CGD is calculated by considering five different cases. The first and the second cases, namely $\left|(\Delta s_1)^2 b_{11} b_{21}\right|$ and $\left|(\Delta s_2)^2 b_{12} b_{22}\right|$, have the same output for both $\mathbf{B} = \left[b_{11}^*, b_{12}^*; b_{21}^*, b_{22}^*\right]$ and $\mathbf{B} = \left[b_{11}^*, -b_{12}^*; -b_{21}^*, b_{22}^*\right]$, given the same pairs of modulated symbols $(s_1, s_2) = (t_1, t_2)$ and $(\hat{s}_1, \hat{s}_2) = (\hat{t}_1, \hat{t}_2)$, where $t_1, t_2, \hat{t}_1, \hat{t}_2 \in \mathcal{Z}$. Next, let us consider the third case, namely $|(\Delta s_1 b_{11} + \Delta s_2 b_{12})(\Delta s_1 b_{21} + \Delta s_2 b_{22})|$. It can be found that the resulting CGD for $\mathbf{B} = \left[b_{11}^*, b_{12}^*; b_{21}^*, b_{22}^*\right]$ with any pairs of modulated symbols $(s_1, s_2) = (t_1, t_2)$ and $(\hat{s}_1, \hat{s}_2) = (\hat{t}_1, \hat{t}_2)$, is the same as that for $\mathbf{B} = \left[b_{11}^*, -b_{12}^*; -b_{21}^*, b_{22}^*\right]$ with pairs of modulated symbols $(s_1, s_2) = (t_1, -t_2)$ and $(\hat{s}_1, \hat{s}_2) = (\hat{t}_1, -\hat{t}_2)$. Finally, for the fourth or the fifth case, namely $(s_1 b_{11} + s_2 b_{12})^2$ or $(s_1 b_{21} + s_2 b_{22})^2$, there always exists a pair of modulated symbols $(s_1, s_2) = (t_1, -t_2)$ for $\mathbf{B} = \left[b_{11}^*, -b_{12}^*; -b_{21}^*, b_{22}^*\right]$ that lead to the same CGD as that for $\mathbf{B} = \left[b_{11}^*, b_{12}^*; b_{21}^*, b_{22}^*\right]$ given a pair of modulated symbols $(s_1, s_2) = (t_1, t_2)$. To sum up, the resulting maximum CGD by $\mathbf{B} = \left[b_{11}^*, b_{12}^*; b_{21}^*, b_{22}^*\right]$ can be also achieved by $\mathbf{B} = \left[b_{11}^*, -b_{12}^*; -b_{21}^*, b_{22}^*\right]$, completing the proof. □

Lemma 2: Let us define $g_1(t_1, t_2) = |(t_1 \cos\theta + t_2 \sin\theta)(t_1 \sin\theta + t_2 \cos\theta)|$ and $g_2\left(\hat{t}_1, \hat{t}_2\right) = \left(\hat{t}_1 \cos\theta + \hat{t}_2 \sin\theta\right)^2$, where $t_1, t_2, \hat{t}_1, \hat{t}_2 \in \mathcal{Z}$, $\theta \in (0, \pi/4)$. For any given parameters (t_1, t_2), there always exist parameters $(\hat{t}_1, \hat{t}_2)$, satisfying $g_2\left(\hat{t}_1, \hat{t}_2\right) \leq g_1(t_1, t_2)$.

Proof: Since $g_1(t_1, t_2) = g_1(t_2, t_1)$, it is sufficient to consider the case of $|t_1| \geq |t_2|$. We now prove that when $(\hat{t}_1, \hat{t}_2) = (t_2, t_1)$, it yields $g_2(t_2, t_1) \leq g_1(t_1, t_2)$. Since $g_1(t_1, t_2), g_2(t_2, t_1) > 0$, it is equivalent to prove (35), shown at the top of this page.

Define $\mathbf{t} = [t_1, t_2]$, $\mathbf{e}_1 = [\cos\theta, \sin\theta]$, and $\mathbf{e}_2 = [\sin\theta, \cos\theta]$. Since $\theta \in (0, \pi/4)$, it follows that $\cos\theta > \sin\theta > 0$, and for $|t_1| \geq |t_2|$, $|\cos\langle \mathbf{t}, \mathbf{e}_1\rangle| \geq |\cos\langle \mathbf{t}, \mathbf{e}_2\rangle|$. Therefore, $(t_1 \sin\theta + t_2 \cos\theta)^2 - (t_1 \cos\theta + t_2 \sin\theta)^2 = |\mathbf{t} \cdot \mathbf{e}_2|^2 - |\mathbf{t} \cdot \mathbf{e}_1|^2 \leq 0$, completing the proof □

Proposition: Two different types of linear precoders, Type I and Type II, lead to the maximum CGD, whose outputs are a point of a rotated M^2-QAM constellation for Type I and a point of a diamond-shaped M^2-QAM constellation for Type II, and the corresponding precoding coefficients are given by

$$\begin{aligned} b_{11}^* &= \pm\cos p(M), \quad b_{12}^* = \pm\sin p(M) \\ b_{21}^* &= \pm\sin p(M), \quad b_{22}^* = \pm\cos p(M) \end{aligned} \tag{36}$$

with (37), shown at the bottom of the next page, where $b_{11}^* b_{12}^* b_{21}^* b_{22}^* < 0$ for Type I and $b_{11}^* b_{12}^* b_{21}^* b_{22}^* > 0$ for Type II.

Proof: Since the symbols s_1 and s_2 are drawn from the regular M-PAM constellation, it can be inferred from (34) that $|b_{11}^*| = |b_{22}^*|$ and $|b_{12}^*| = |b_{21}^*|$ due to the symmetry. According to *Lemma 1*, it is sufficient to consider $b_{11}^*, b_{12}^*, b_{21}^*, b_{22}^* > 0$. Further, since swapping b_{11}^* and b_{12}^* as well as b_{21}^* and b_{22}^*

TABLE III
OPTIMAL PRECODING MATRICES FOR $M = 2$, 4, AND 8

M	2	4	8
Type I ($\mathbf{B}_{opt}$)	$\begin{bmatrix} 0.9856 & -0.1691 \\ 0.1691 & 0.9856 \end{bmatrix}$	$\begin{bmatrix} 0.9939 & 0.1104 \\ 0.1104 & -0.9939 \end{bmatrix}$	$\begin{bmatrix} 0.9977 & 0.0681 \\ 0.0681 & -0.9977 \end{bmatrix}$
Type II ($\mathbf{B}_{opt}$)	$\begin{bmatrix} 0.9856 & -0.1691 \\ -0.1691 & 0.9856 \end{bmatrix}$	$\begin{bmatrix} 0.9939 & 0.1104 \\ 0.1104 & 0.9939 \end{bmatrix}$	$\begin{bmatrix} 0.9977 & -0.0681 \\ -0.0681 & 0.9977 \end{bmatrix}$

results in the same CGD, it is sufficient to consider the case of $b_{11}^* > b_{12}^*$.

Let $b_{11}^* = \cos\theta_{opt}, b_{12}^* = \sin\theta_{opt}$, $\theta_{opt} \in (0, \pi/4)$. Since $\Delta s_1, \Delta s_2 \in \{\pm 2, \pm 4 \ldots, \pm 2(M-1)\}$, the optimization problem in (34) can be equivalently formulated as (38), shown at the bottom of the next page.

According to *Lemma 2*, there always exist pairs of modulated symbols (s_1, s_2) and $(\hat{s}_1, \hat{s}_2)$, satisfying $|(\Delta s_1 \cos\theta + \Delta s_2 \sin\theta)(\Delta s_1 \sin\theta + \Delta s_2 \cos\theta)| \geq 4(s_1 \cos\theta + s_2 \sin\theta)^2$. Therefore, (38) can be further simplified as

$$\theta_{opt} = \arg\max_{\theta} \left\{ \min \left\{ 4\cos\theta \sin\theta, (s_1 \cos\theta + s_2 \sin\theta)^2 \right\} \right\}, \quad s.t.\ \theta \in (0, \pi/4). \tag{39}$$

Recall that $s_1, s_2 \in \mathcal{Z}(= \{\pm 1, \pm 3, \pm(M-1)\})$ and $\theta \in (0, \pi/4)$. It can be readily figured out that the solution to (39) satisfies

$$4\cos\theta_{opt} \sin\theta_{opt} = \left(\cos\theta_{opt} - (M-1)\sin\theta_{opt}\right)^2. \tag{40}$$

Solving (40) yields $\sin 2\theta_{opt} = p(M)$, where $p(M)$ is given by (37).

As revealed in *Lemma 1*, the signs of the four precoding coefficients can be arbitrary, and thus 16 precoders can be obtained. However, it can be found that these 16 precoders can be classified into two types corresponding to the value of the product of the signs. Specifically, if the value is negative, the output of the precoder belongs to a rotated M^2-QAM constellation; otherwise, it belongs to a point of a diamond-shaped M^2-QAM constellation, completing the proof. □

For convenience of practical implementation, we present the exact values of the optimal precodering matrices for $M = 2$, 4, and 8 in Table III. To better understand how the two types of the linear precoders perform, we take $M = 2$ and 4 as an example and depict the resulting outputs in Figs. 4(a) and (b), respectively. Fig. 4, which contains rotated and diamond-shaped constellations, also verifies the *Proposition*.

The *Proposition* shows that to achieve a diversity order of two, instead of transmitting an M-PAM symbol over the I/Q- branch of a subcarrier, we can generate a pair of symbols from a rotated or diamond-shaped M^2-QAM constellation and transmit their real and imaginary parts over the I/Q- branch of an active subcarrier pair. From this aspect, the Type I precoding method is exactly the CIOD method applying to the I/Q- branch. However, we note that different optimal rotation angles are obtained when applying the CIOD method to OFDM-IM and OFDM-HIQ-IM (or OFDM-IQ-IM) systems due to different objective functions. For example, the optimal rotation angles for 4-, 16-, and 64−QAM constellations, respectively, in OFDM-IM systems are 15°, 8.5°, and 4.5° [39], while in OFDM-HIQ-IM/OFDM-IQ-IM systems, are 9.7°, 6.3°, and 4°.

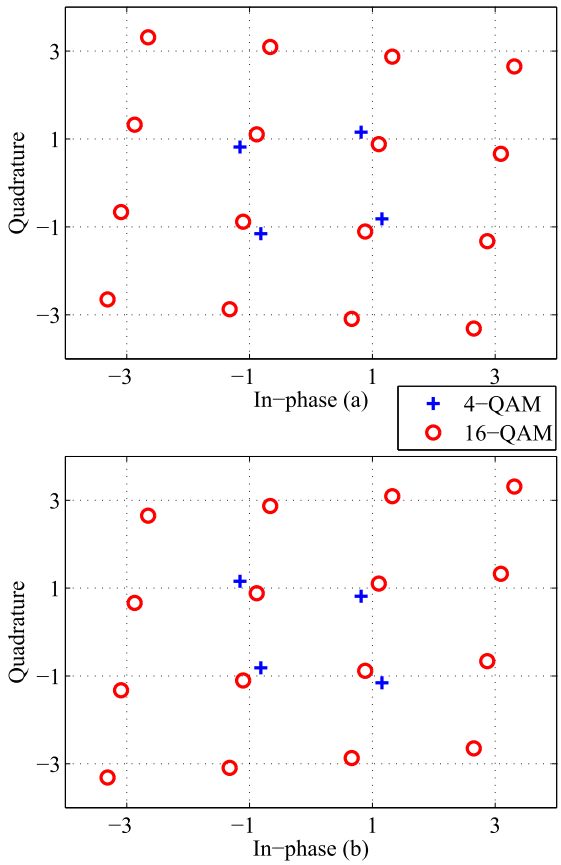

Fig. 4. The outputs of the optimal linear precoders for $M = 2$ and 4: (a) Type I; (b) Type II.

$$p(M) = \frac{1}{2} \arcsin \frac{2(M+1)\left(M^2 - 2M + 2\right) - 4(M-2)\sqrt{M^3}}{(M-1)^4 + 2(M-1)^2 + 16(M-1) + 17} \tag{37}$$

TABLE IV

RECEIVER COMPLEXITY COMPARISON BETWEEN LP-OFDM-IQ-IM, OFDM-HIQ-IM, AND CLASSICAL OFDM-IM

System Setup	LP-OFDM-IQ-IM		OFDM-HIQ-IM		Classical OFDM-IM	
	ML	LLR	ML	LLR	ML	LLR
S1	2048	68	1024	8	192	16
S2	342	19	342	4	43	8
S3	32768	72	16384	8	192	16
S4	24576	304	6144	16	768	64

C. Receiver Complexity and Performance Analysis

By focusing on the receiver end and considering both optimal ML and LLR detection, we compare the computational complexity of LP-OFDM-IQ-IM with that of classical OFDM-IM. The following four system setups are considered for comparison:

- S1: $(8, 2, 2)$, 4-PAM for proposed schemes, and $(8, 3)$, 16-QAM for classical OFDM-IM;
- S2: $(6, 4, 4)$, 2-PAM for proposed schemes, and $(6, 4)$, 8-QAM for classical OFDM-IM;
- S3: $(8, 4, 4)$, 4-PAM for proposed schemes, and $(8, 6)$, 16-QAM for classical OFDM-IM;
- S4: $(8, 6, 6)$, 8-PAM for proposed schemes, and $(8, 6)$, 64-QAM for classical OFDM-IM.

For each system setup, the same SE is achieved, ensuring a relatively fair comparison. Specifically, the corresponding SE values for S1, S2, S3, and S4 setups are 2.125 bps/Hz, 2.5 bps/Hz, 3.5 bps/Hz, and 8.625 bps/Hz, respectively. Considering the average number of metric calculations per subcarrier as a performance metric, we summarize the comparison results in Table IV, where the complexity values corresponding to LP-OFDM-IQ-IM and classical OFDM-IM with the optimal ML detection are, respectively, calculated by $2^{p_1}M^2(k^I + k^Q)/2n$ and $2^{p_1}kM/n$, while those with the LLR detection, are, respectively, calculated by $M^2[4+(k^I+k^Q)/2n]$ and M. As a reference, the OFDM-HIQ-IM scheme is also added in Table IV, whose computational complexity has been analyzed in Section III.C. From Table IV, we observe that the computational complexity of the LLR detection of LP-OFDM-IQ-IM is significantly lower than that of the optimal ML detection, though it is still higher than that of the other two schemes due to pair-by-pair searching. However, we note that this price is worth considering its superior performance, as will be verified in Section V. In addition, it can be found from Table IV that for LLR detection, OFDM-HIQ-IM even has a lower computational complexity than classical OFDM-IM. This is understandable since with the same subcarrier activation parameters, classical OFDM conveys fewer IM bits than OFDM-HIQ-IM, and the resulting SE loss has to be compensated by using a higher-order signal constellation, which determines the computational complexity of the LLR detector for both schemes.

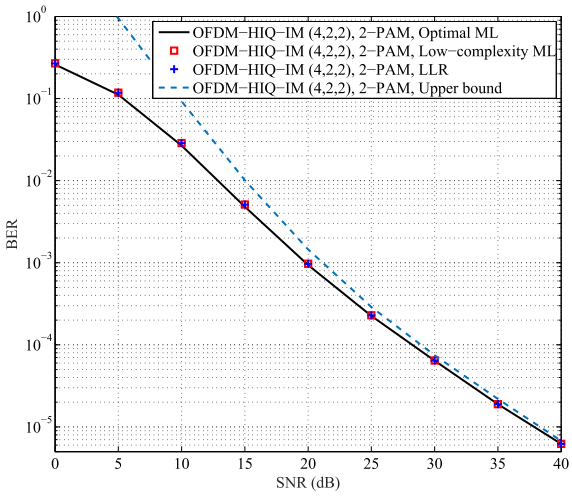

Fig. 5. Performance comparison between LLR, low-complexity ML, and ML detectors of OFDM-HIQ-IM, where the system parameters are $(n, k^I, k^Q) = (4, 2, 2)$ and 2-PAM is used on both I- and Q- branches.

On the other hand, in analogy with the analytical methodology in Section III.D, we can easily derive an asymptotically tight upper bound on the BER and the achievable rate of the LP-OFDM-IQ-IM system, which can be shown to have the same forms as (21) and (24), respectively. However, attention must be paid to the realizations of $\mathbf{X}_\beta$ for LP-OFDM-IQ-IM, whose diagonal elements should be determined by the outputs of the linear precoders on both I- and Q- branches as well as the joint IQ index mapper.

V. SIMULATION RESULTS AND COMPARISONS

In this section, Monte Carlo simulations are conducted to examine the performances of OFDM-HIQ-IM and LP-OFDM-IQ-IM. In the simulations, the number of total OFDM subcarriers is $N = 128$ and the length of CP is $N/4 = 32$. The wireless channel is modeled by an exponentially decaying power delay profile with 16 taps, where each tap is generated according to Rayleigh distribution. The uncoded BER and achievable rate are chosen as performance metrics and evaluated versus the receive SNR per subcarrier.

A. Performance of OFDM-HIQ-IM

In this subsection, we evaluate the performance of OFDM-HIQ-IM.

To see how the two proposed low-complexity detectors perform and to verify the tightness of the proposed BER upper bound, we assume OFDM-HIQ-IM systems with $(n, k^I, k^Q) = (4, 2, 2)$ and 2-PAM modulation on both I- and Q- branches in Fig. 5. As seen from Fig. 5, the BER performances of the LLR detector and the low-complexity ML detector are negligibly worse than that of the optimal ML detector in the low SNR region and all three detectors

$$\theta_{opt} = \arg\max_{\theta} \left\{ \min \left\{ \begin{array}{l} 4\cos\theta\sin\theta, (s_1\cos\theta + s_2\sin\theta)^2, \\ |(\Delta s_1\cos\theta + \Delta s_2\sin\theta)(\Delta s_1\sin\theta + \Delta s_2\cos\theta)| \end{array} \right\} \right\} \quad s.t. \quad \theta \in (0, \pi/4). \tag{38}$$

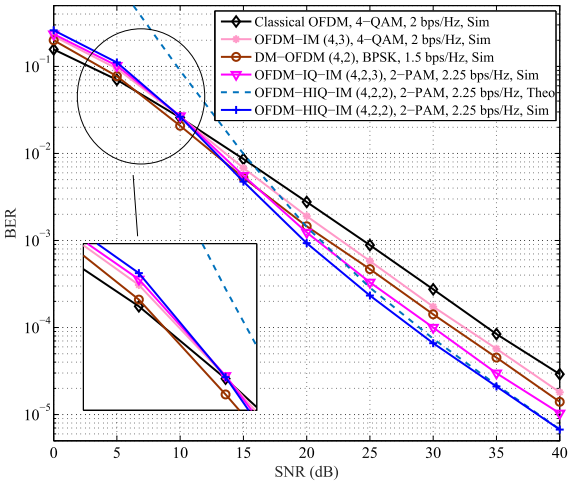

Fig. 6. BER performance comparison among classical OFDM, OFDM-IM, DM-OFDM, OFDM-IQ-IM, and OFDM-HIQ-IM, where classical OFDM employs 4-QAM, OFDM-IM with $(n, k) = (4, 2)$ employs 4-QAM, DM-OFDM with $(n, k) = (4, 2)$ employs BPSK and $\pi/2$-rotated BPSK for the primary and secondary constellations, respectively, OFDM-IQ-IM with $(n, k^I, k^Q) = (4, 2, 3)$ employs 2-PAM on both I- and Q- branches, and OFDM-HIQ-IM with $(n, k^I, k^Q) = (4, 2, 2)$ employs 2-PAM on both branches.

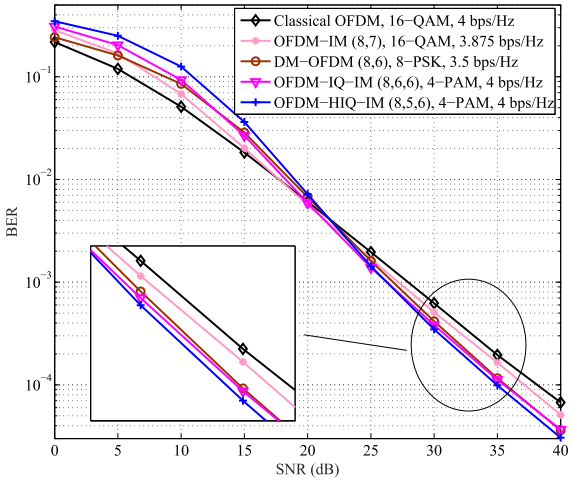

Fig. 7. BER performance comparison among classical OFDM, OFDM-IM, DM-OFDM, OFDM-IQ-IM, and OFDM-HIQ-IM, where classical OFDM employs 16-QAM, OFDM-IM with $(n, k) = (8, 7)$ employs 16-QAM, DM-OFDM with $(n, k) = (8, 6)$ employs 8-PSK and $\pi/8$-rotated 8-PSK for the primary and secondary constellations, respectively, OFDM-IQ-IM with $(n, k^I, k^Q) = (8, 6, 6)$ employs 4-PAM on both I- and Q- branches, and OFDM-HIQ-IM with $(n, k^I, k^Q) = (8, 5, 6)$ employs 4-PAM on both branches.

perform the same in the medium-to-high SNR region. This can be understood by the fact that at low SNR, both low-complexity detectors may decide on the illegitimate active indices combinations with a very small probability (in this system setup, the proportion of the illegitimate active indices combinations is $4/36 = 11.1\%$) and at medium-to-high SNR, the errors mainly stem from the ordinary modulation bits, when there is no difference between three detectors. Though it is not shown in this paper, we observe a similar phenomenon for several different system setups. Therefore, the two proposed low-complexity detectors are much preferred in practical use for their near-ML performance and significantly reduced computational complexity. On the other hand, we observe that the proposed upper bound in (21) is considerably tight in the high SNR region, which verifies the feasibility of the independence assumption for the analysis of the upper bound on the BER of OFDM-HIQ-IM systems.

In Figs. 6 and 7, we compare the BER performance of OFDM-HIQ-IM with that of OFDM-IQ-IM [25], where their SEs are equated to be 2.25 and 4 bps/Hz, respectively. Specifically, for 2.25 bps/Hz, both OFDM-IQ-IM and OFDM-HIQ-IM employ 2-PAM on both I- and Q- branches with the system setups chosen as $(4, 2, 3)$ and $(4, 2, 2)$, respectively, while for 4 bps/Hz, they employ 4-PAM on both branches with the system setups chosen as $(8, 6, 6)$ and $(8, 5, 6)$, respectively. The classical OFDM, OFDM-IM [24], and DM-OFDM [32] systems are also considered for comparison, where for the classical OFDM system we assume 4-QAM and 16-QAM, for the OFDM-IM system we assume $(n, k) = (4, 3)$ with 4-QAM and $(8, 7)$ with 16-QAM, and for the DM-OFDM system we assume $(n, k) = (4, 2)$ with (BPSK, $\pi/2$-rotated BPSK) and $(8, 6)$ with (8-PSK, $\pi/8$-rotated 8-PSK) in Figs. 6 and 7, respectively. Note that in Fig. 6, the classical OFDM and OFDM-IM systems attain 2 bps/Hz while the DM-OFDM system achieves 1.5 bps/Hz, and in Fig. 7, the OFDM-IM and DM-OFDM systems achieve 3.875 and 3.5 bps/Hz, respectively. From Fig. 6, we observe that at 2.25 bps/Hz, OFDM-HIQ-IM performs similarly to OFDM-IQ-IM when the SNR is low whilst its superiority becomes apparent as the SNR increases. For example, at high SNRs, about 2dB SNR gain is observed. This gain can be accounted for the one more IM bit due to joint I- and Q- encoding and the improved minimum Euclidean distance due to one less active quadrature component. Compared to classical OFDM and OFDM-IM, OFDM-HIQ-IM achieves about 6dB and 4dB SNR gains at medium-to-high SNR, respectively, despite a higher SE. Due to the enhanced transmit power per active I/Q component transferred from the inactive ones, OFDM-HIQ-IM is superior to DM-OFDM despite they employ the same modulation order for active subcarriers. On the other hand, from Fig. 7, we observe that at 4 bps/Hz, OFDM-HIQ-IM performs worse than OFDM-IQ-IM in the low SNR region; however, it achieves approximately 1dB SNR gain in the high SNR region. This is because the error of IM bits dominates that of the ordinary modulation bits at low SNR while it is the opposite at high SNR. The reason for the smaller SNR gain is that as the SE becomes larger, the proportion of the ordinary modulation bits becomes higher and meanwhile, the power gain due to subcarrier inactivation becomes smaller. Since the advantages of IM for much higher SEs are limited [28], OFDM-HIQ-IM is favorable in this sense. For the same reason described earlier, OFDM-HIQ-IM outperforms DM-OFDM in spite of a much larger SE. It is worth noting that by leveraging the numbers of IM and ordinary modulation bits, OFDM-HIQ-IM and DM-OFDM can have comparable computational complexity, since the former has more number of IM bits while the latter has more number of ordinary modulation bits for the same system configuration.

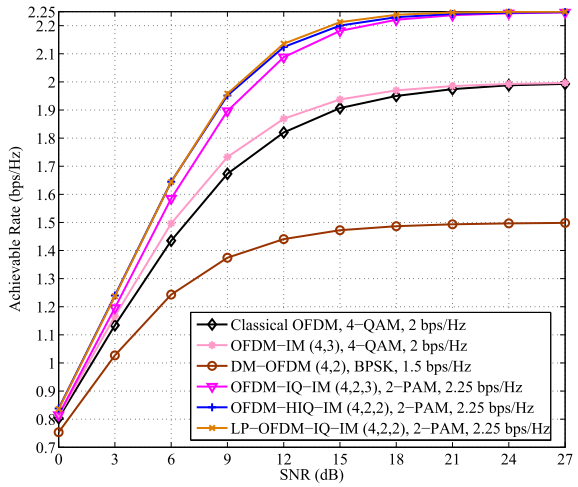

Fig. 8. Comparison of the achievable rates of classical OFDM, OFDM-IM, DM-OFDM, OFDM-IQ-IM, OFDM-HIQ-IM, and LP-OFDM-IQ-IM, where classical OFDM employs 4-QAM, OFDM-IM with $(n, k) = (4, 2)$ employs 4-QAM, DM-OFDM with $(n, k) = (4, 2)$ employs BPSK and $\pi/2$-rotated BPSK for the primary and secondary constellations, respectively, OFDM-IQ-IM with $(n, k^I, k^Q) = (4, 2, 3)$ employs 2-PAM on both I- and Q- branches, OFDM-HIQ-IM with $(n, k^I, k^Q) = (4, 2, 2)$ employs 2-PAM on both branches, and LP-OFDM-IQ-IM adopts the Type I precoder with the same system parameters as OFDM-HIQ-IM.

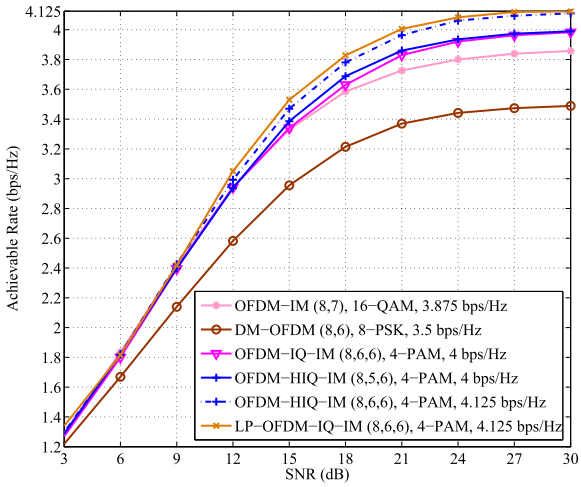

Fig. 9. Achievable rate performance comparison between OFDM-IM, DM-OFDM, OFDM-IQ-IM, OFDM-HIQ-IM, and LP-OFDM-IQ-IM, where OFDM-IM with $(n, k) = (8, 7)$ employs 16-QAM, DM-OFDM with $(n, k) = (8, 6)$ employs 8-PSK and $\pi/8$-rotated 8-PSK for the primary and secondary constellations, respectively, OFDM-IQ-IM with $(n, k^I, k^Q) = (8, 6, 6)$ employs 4-PAM on both I- and Q- branches, OFDM-HIQ-IM with $(n, k^I, k^Q) = (8, 5, 6)/(8, 6, 6)$ employs 4-PAM on both branches, and LP-OFDM-IQ-IM adopts the Type II precoder based on the OFDM-HIQ-IM system with $(n, k^I, k^Q) = (8, 6, 6)$ and 4-PAM on both branches.

The achievable rates of OFDM-HIQ-IM schemes at SEs of 2.25 and 4 bps/Hz are evaluated in Figs. 8 and 9, respectively, where their system parameters and competitors are chosen to be the same as those in Figs. 6 and 7. For clarity, the curve of classical OFDM is removed in Fig. 9. As seen from Figs. 8 and 9, the achievable rates of all systems saturate at their corresponding uncoded transmitted information rates, namely SEs, at very high SNR. This is reasonable since in both cases, the input of the channel is subject to a finite alphabet and the resulting achievable rate is always smaller than the channel capacity. On the other hand, in consistence with the observation in Figs. 6 and 7, OFDM-HIQ-IM also outperforms OFDM-IQ-IM in terms of the achievable rate. Similarly, this can be accounted for the stronger protection of the IM bits than the ordinary modulation bits. Therefore, we are led to the conclusion that OFDM-HIQ-IM is more favorable than OFDM-IQ-IM for both uncoded and coded transmission. However, the price paid for this improvement is a very little decoding delay, which can be ensured by the two proposed low-complexity detectors in Section III.C.

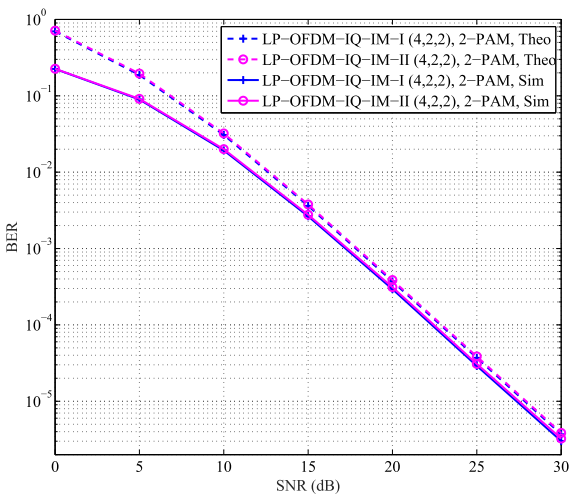

Fig. 10. Performance comparison between Type I and Type II precoders of OFDM-IQ-IM, where the system parameters are $(n, k^I, k^Q) = (4, 2, 2)$ and 2-PAM is used on both I- and Q- branches.

B. Performance of LP-OFDM-IQ-IM

In this subsection, we evaluate the performance of LP-OFDM-IQ-IM.

In Fig. 10, the OFDM-IQ-IM system with $(4, 2, 2)$ and 2-PAM modulation on both I- and Q- branches is considered for BER performance comparison between the Type I and Type II precoders, denoted by LP-OFDM-IQ-IM-I and LP-OFDM-IQ-IM-II, respectively, where the rotation angle for LP-OFDM-IQ-IM-I is chosen as the optimal one, i.e., 9.7° for this system setup, and the BER upper bounds calculated from (21) are also depicted for reference. It can be observed from Fig. 10 that LP-OFDM-IQ-IM-I exhibits negligible superiority over LP-OFDM-IQ-IM-II in the entire SNR region. This small difference is due to the max-min criterion we follow in (32), which does not take into account all PEPs that decrease with the square of SNR. Due to their similar performance, in the sequel, we take either the Type I or Type II precoder as a representative for performance comparison with other schemes.

Fig. 11 compares the BER performances of OFDM-HIQ-IM systems with and without LCP at 2.25 bps/Hz, where the Type I precoder with a rotation angle of 9.7° is assumed, the system parameters are chosen as $(4, 2, 2)$, and 2-PAM is used on both I- and Q- branches. The BER curves of the classical OFDM system with 4-QAM, the LCP aided OFDM-IM (LP-OFDM-IM) system with $(n, k) = (4, 3)$ and

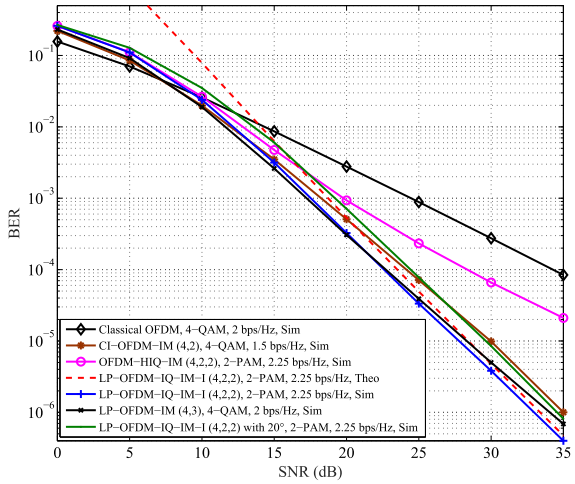

Fig. 11. BER performance comparison among classical OFDM, CI-OFDM-IM, OFDM-HIQ-IM, LP-OFDM-IM, and LP-OFDM-IQ-IM, where classical OFDM employs 4-QAM, CI-OFDM-IM with $(n, k) = (4, 2)$ employs 4-QAM with 15° rotation, OFDM-HIQ-IM with $(n, k^I, k^Q) = (4, 2, 2)$ employs 2-PAM on both I- and Q- branches, LP-OFDM-IM with $(n, k) = (4, 3)$ employs 4-QAM, and LP-OFDM-IQ-IM adopts the Type I precoder based on the OFDM-HIQ-IM system with $(n, k^I, k^Q) = (4, 2, 2)$, 2-PAM on both branches, and a rotation angle of 9.7°/20°.

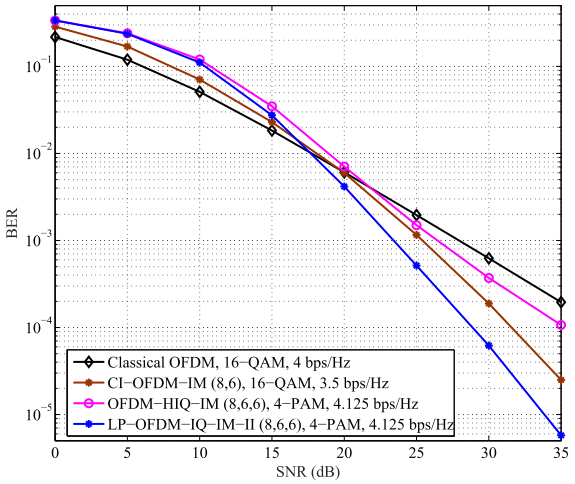

Fig. 12. BER performance comparison among classical OFDM, CI-OFDM-IM, OFDM-HIQ-IM, and LP-OFDM-IQ-IM, where classical OFDM employs 16-QAM, CI-OFDM-IM with $(n, k) = (8, 6)$ employs 16-QAM with 8.5° rotation, OFDM-HIQ-IM with $(n, k^I, k^Q) = (8, 6, 6)$ employs 4-PAM on both I- and Q- branches, and LP-OFDM-IQ-IM adopts the Type II precoder based on the OFDM-HIQ-IM system with $(n, k^I, k^Q) = (8, 6, 6)$ and 4-PAM on both branches.

4-QAM, in which the LCP method for OFDM systems [41] is directly applied to the OFDM-IM framework, and the coordinate interleaved OFDM-IM (CI-OFDM-IM) [39] system with $(n, k) = (4, 2)$ and 4-QAM are also added for BER comparison, where the first two systems achieve 2 bps/Hz while the last system 1.5 bps/Hz. The rotation angle for the CI-OFDM-IM system is 15° [39]. To examine the sensitivity of LP-OFDM-IQ-IM-I to the rotation angle, we further consider LP-OFDM-IQ-IM-I with a random rotation angle of 20° in Fig. 11. From Fig. 11, we notice that as similar to the aforementioned cases, all index modulated systems perform worse than the classical OFDM system at low SNR due to the dominant errors caused by the SAP mismatch, while they become overwhelming for a higher SNR due to a stronger protection of the IM bits. However, among them, the CI-OFDM-IM, LP-OFDM-IM, and LP-OFDM-IQ-IM-I systems exhibit a faster BER decline as the protection of the ordinary modulation bits is further strengthened. Moreover, it is observed that LP-OFDM-IQ-IM-I exhibits approximately 2.5dB and 1dB SNR gains over CI-OFDM-IM and LP-OFDM-IM at high SNR, respectively, despite a larger SE, which can be explained by the improved minimum Euclidean distance from the I/Q IM. On the other hand, we find that a noticeable BER performance loss would be incurred when LP-OFDM-IQ-IM-I adopts a random rotation angle different from the optimal one. For example, as shown in Fig. 11, a rotation angle of 20° leads to a loss of approximately 2dB SNR compared with the optimal rotation angle of 9.7°.

BER performance comparison between OFDM-HIQ-IM systems with and without LCP at 4.125 bps/Hz is performed in Fig. 12, where the Type II precoder is assumed, the system parameters are chosen as $(8, 6, 6)$, and 4-PAM is used on both I- and Q- branches. For classical OFDM, 16-QAM is employed, and for CI-OFDM-IM, the system parameters are chosen as $(8, 6)$ and 16-QAM with a rotation angle of 8.5° [39]. Note that in such system setup, CI-OFDM-IM systems have an SE of 3.5 bps/Hz. As can be observed from Fig. 12, LP-OFDM-IQ-IM-II performs best in the high SNR region and advances the intersection point with classical OFDM by about 4dB compared with OFDM-HIQ-IM. On the other hand, we observe similarly that LP-OFDM-IQ-IM-II still outperforms CI-OFDM-IM even though it has a much higher SE.

VI. Conclusion

In this paper, we have proposed OFDM-HIQ-IM and LP-OFDM-IQ-IM to improve the SE and the asymptotic BER performance of OFDM-IM systems, respectively. The two proposed schemes can be further combined to harvest both of their advantages. OFDM-HIQ-IM explores the I- and Q- active components jointly for IM, doubling the IM bits of OFDM-IM and transmitting one more IM bit than OFDM-IQ-IM in most cases. An asymptotically tight upper bound has been derived and two low-complexity near-optimal detectors have been designed for OFDM-HIQ-IM. LP-OFDM-IQ-IM combines a pair of I/Q- symbols linearly, achieving an additional diversity gain over OFDM-IM, OFDM-IQ-IM, and OFDM-HIQ-IM. Two different optimal linear combination methods in the sense of maximizing the minimum CGD have been found, which result in the rotation and compression of the M^2-QAM constellation, respectively. The precoding coefficients for both methods have been derived analytically and the low-complexity LLR detector has been designed for LP-OFDM-IQ-IM. Monte Carlo simulations have been conducted and results have verified the analysis and the advantages of OFDM-HIQ-IM and LP-OFDM-IQ-IM over classical OFDM as well as existing OFDM-IM schemes.

References

[1] M. Wen, X. Cheng, and L. Yang, *Index Modulation for 5G Wireless Communications (Wireless Networks)*. Berlin, Germany: Springer, 2017.

[2] E. Basar, "Index modulation techniques for 5G wireless networks," *IEEE Commun. Mag.*, vol. 54, no. 7, pp. 168–175, Jul. 2016.

[3] R. Mesleh, H. Haas, S. Sinanovic, C. Ahn, and S. Yun, "Spatial modulation," *IEEE Trans. Veh. Technol.*, vol. 57, no. 4, pp. 2228–2242, Jul. 2008.

[4] M. Di Renzo, H. Haas, and P. M. Grant, "Spatial modulation for multiple-antenna wireless systems: A survey," *IEEE Commun. Mag.*, vol. 49, no. 12, pp. 182–191, Dec. 2011.

[5] M. Di Renzo, H. Haas, A. Ghrayeb, S. Sugiura, and L. Hanzo, "Spatial modulation for generalized MIMO: Challenges, opportunities and implementation," *Proc. IEEE*, vol. 102, no. 1, pp. 56–103, Jan. 2014.

[6] A. Younis, N. Serafimovski, R. Mesleh, and H. Haas, "Generalised spatial modulation," in *Proc. IEEE Asilomar Conf. Signals, Syst. Comput.*, Pacific Grove, CA, USA, Nov. 2010, pp. 1498–1502.

[7] J. Wang, S. Jia, and J. Song, "Generalised spatial modulation system with multiple active transmit antennas and low complexity detection scheme," *IEEE Trans. Wireless Commun.*, vol. 11, no. 4, pp. 1605–1615, Apr. 2012.

[8] R. Mesleh, S. Ikki, and H. M. Aggoune, "Quadrature spatial modulation," *IEEE Trans. Veh. Technol.*, vol. 64, no. 6, pp. 2738–2742, Jun. 2015.

[9] J. Li, M. Wen, X. Cheng, Y. Yan, S. Song, and M. H. Lee, "Generalised pre-coding aided quadrature spatial modulation," *IEEE Trans. Veh. Technol.*, vol. 66, no. 2, pp. 1881–1886, Feb. 2017.

[10] C.-C. Cheng, H. Sari, S. Sezginer, and Y. T. Su, "Enhanced spatial modulation with multiple signal constellations," *IEEE Trans. Commun.*, vol. 63, no. 6, pp. 2237–2248, Jun. 2015.

[11] E. Basar, U. Aygolu, E. Panayirci, and H. V. Poor, "Space-time block coded spatial modulation," *IEEE Trans. Commun.*, vol. 59, no. 3, pp. 823–832, Mar. 2011.

[12] R. Rajashekar and K. V. S. Hari, "Modulation diversity for spatial modulation using complex interleaved orthogonal design," in *Proc. IEEE TENCON*, Cebu, Philippines, Nov. 2012, pp. 1–6.

[13] S. M. Alamouti, "A simple transmit diversity technique for wireless commmunications," *IEEE J. Sel. Areas Commun.*, vol. 16, no. 8, pp. 1451–1458, Oct. 1998.

[14] K. Boulle and J. C. Belfiore, "Modulation schemes designed for the Rayleigh channel," in *Proc. Conf. Inf. Sci. Syst.*, Princeton, NJ, USA, pp. 288–293,

[15] J. Boutrous and E. Viterbo, "Signal space diversity: A power- and bandwidth-efficient diversity technique for the Rayleigh fading channel," *IEEE Trans. Inf. Theory*, vol. 44, no. 4, pp. 1453–1467, Jul. 1998.

[16] K. V. Srinivas, R. D. Koilpillai, S. Bhashyam, and K. Giridhar, "Co-ordinate interleaved spatial multiplexing with channel state information," *IEEE Trans. Wireless Commun.*, vol. 8, no. 6, pp. 2755–2762, Jun. 2009.

[17] M. Z. Ali Khan and B. S. Rajan, "Single-symbol maximum likelihood decodable linear STBCs," *IEEE Trans. Inf. Theory*, vol. 52, no. 5, pp. 2062–2091, May 2006.

[18] C. Yuen, Y. L. Guan, and T. T. Tjhung, "Quasi-orthogonal STBC with minimum decoding complexity," *IEEE Trans. Wireless Commun.*, vol. 4, no. 5, pp. 2089–2094, Sep. 2005.

[19] P. Yang, M. Di Renzo, Y. Xiao, S. Li, and L. Hanzo, "Design guidelines for spatial modulation," *IEEE Commun. Surveys. Tuts.*, vol. 17, no. 1, pp. 6–26, 1st Quart., 2015.

[20] P. Yang *et al.*, "Single-carrier SM-MIMO: A promising design for broadband large-scale antenna systems," *IEEE Commun. Surveys. Tuts.*, vol. 18, no. 3, pp. 1687–1716, 3rd Quart., 2016.

[21] P. K. Frenger and N. A. B. Svensson, "Parallel combinatory OFDM signaling," *IEEE Trans. Commun.*, vol. 47, no. 4, pp. 558–567, Apr. 1999.

[22] R. Abu-Alhiga and H. Haas, "Subcarrier-index modulation OFDM," in *Proc. IEEE 20th Int. Symp. Pers., Indoor Mobile Radio Commun. (PIMRC)*, Tokyo, Japan, Sep. 2009, pp. 177–181.

[23] D. Tsonev, S. Sinanovic, and H. Haas, "Enhanced subcarrier index modulation (SIM) OFDM," in *Proc. IEEE Global Commun. Conf. (GLOBECOM) Workshops*, Houston, TX, USA, Dec. 2011, pp. 728–732.

[24] E. Basar, U. Aygolu, E. Panayirci, and H. V. Poor, "Orthogonal frequency division multiplexing with index modulation," *IEEE Trans. Signal Process.*, vol. 61, no. 22, pp. 5536–5549, Nov. 2013.

[25] B. Zheng, F. Chen, M. Wen, F. Ji, H. Yu, and Y. Liu, "Low-complexity ML detector and performance analysis for OFDM with in-phase/quadrature index modulation," *IEEE Commun. Lett.*, vol. 19, no. 11, pp. 1893–1896, Nov. 2015.

[26] M. Wen, X. Cheng, M. Ma, B. Jiao, and H. V. Poor, "On the achievable rate of OFDM with index modulation," *IEEE Trans. Signal Process.*, vol. 64, no. 8, pp. 1919–1932, Apr. 2016.

[27] M. Wen, X. Cheng, and L. Yang, "Optimizing the energy efficiency of OFDM with index modulation," in *Proc. IEEE Int. Conf. Commun. Syst. (ICCS)*, Nov. 2014, pp. 31–35.

[28] N. Ishikawa, S. Sugiura, and L. Hanzo, "Subcarrier-index modulation aided OFDM-will it work?" *IEEE Access*, vol. 4, pp. 2580–2593, 2016.

[29] Q. Ma, P. Yang, Y. Xiao, H. Bai, and S. Li, "Error probability analysis of OFDM-IM with carrier frequency offset," *IEEE Commun. Lett.*, vol. 20, no. 12, pp. 2434–2437, Dec. 2016.

[30] M. Wen, X. Cheng, L. Yang, Y. Li, X. Cheng, and F. Ji, "Index modulated OFDM for underwater acoustic communications," *IEEE Commun. Mag.*, vol. 54, no. 5, pp. 132–137, May 2016.

[31] R. Fan, Y. J. Yu, and Y. L. Guan, "Generalization of orthogonal frequency division multiplexing with index modulation," *IEEE Trans. Wireless Commun.*, vol. 14, no. 10, pp. 5350–5359, Oct. 2015.

[32] T. Mao, Z. Wang, Q. Wang, S. Chen, and L. Hanzo, "Dual-mode index modulation aided OFDM," *IEEE Access*, vol. 5, pp. 50–60, 2017.

[33] E. Basar, "Multiple-input multiple-output OFDM with index modulation," *IEEE Signal Process. Lett.*, vol. 22, no. 12, pp. 2259–2263, Dec. 2015.

[34] E. Basar, "On multiple-input multiple-output OFDM with index modulation for next generation wireless networks," *IEEE Trans. Signal Process.*, vol. 64, no. 15, pp. 3868–3878, Aug. 2016.

[35] B. Zheng, M. Wen, E. Basar, and F. Chen, "Multiple-input multiple-output OFDM with index modulation: Low-complexity detector design," *IEEE Trans. Signal Process.*, vol. 65, no. 11, pp. 2758–2772, Jun. 2017.

[36] T. Datta, H. S. Eshwaraiah, and A. Chockalingam, "Generalized space-and-frequency index modulation," *IEEE Trans. Veh. Technol.*, vol. 65, no. 7, pp. 4911–4924, Jul. 2016.

[37] Y. Xiao, S. Wang, L. Dan, X. Lei, P. Yang, and W. Xiang, "OFDM with interleaved subcarrier-index modulation," *IEEE Commun. Lett.*, vol. 18, no. 8, pp. 1447–1450, Aug. 2014.

[38] X. Cheng, M. Wen, L. Yang, and Y. Li, "Index modulated OFDM with interleaved grouping for V2X communications," in *Proc. IEEE 17th Int. Conf. Intell. Transp. Syst. (ITSC)*, Oct. 2014, pp. 1097–1104.

[39] E. Basar, "OFDM with index modulation using coordinate interleaving," *IEEE Wireless Commun. Lett.*, vol. 4, no. 4, pp. 381–384, Aug. 2015.

[40] L. Wang, Z. Chen, Z. Gong, and M. Wu, "Space-frequency coded index modulation with linear-complexity maximum likelihood receiver in MIMO-OFDM system," *IEEE Signal Process. Lett.*, vol. 23, no. 10, pp. 1439–1443, Oct. 2016.

[41] Z. Liu, Y. Xin, and G. B. Giannakis, "Linear constellation precoding for OFDM with maximum multipath diversity and coding gains," *IEEE Trans. Commun.*, vol. 51, no. 3, pp. 416–427, Mar. 2003.

[42] N. H. Tran, H. H. Nguyen, and T. Le-Ngoc, "Subcarrier grouping for OFDM with linear constellation precoding over multipath fading channels," *IEEE Trans. Veh. Technol.*, vol. 56, no. 6, pp. 3607–3613, Sep. 2007.

[43] B. T. Vo, H. H. Nguyen, and N. Quoc-Tuan, "Spatial modulation for OFDM with linear constellation precoding," in *Proc. Int. Conf. Adv. Technol. Commun. (ATC)*, Ho Chi Minh City, Vietnam, Oct. 2015, pp. 226–230.

Miaowen Wen (M'14) received the B.S. degree from Beijing Jiaotong University, Beijing, China, in 2009, and the Ph.D. degree from Peking University, Beijing, in 2014. From 2012 to 2013, he was a Visiting Student Research Collaborator with Princeton University, Princeton, NJ, USA. Since 2014, he has been a faculty member with the South China University of Technology, Guangzhou, China. He has authored one book and over 50 papers in refereed journals and conference proceedings. His research interests include index modulation and nonorthogonal multiple access techniques.

Dr. Wen received the Best Paper Award from the IEEE International Conference on Intelligent Transportation Systems Telecommunications in 2012, the IEEE International Conference on Intelligent Transportation Systems in 2014, and the IEEE International Conference on Computing, Networking and Communications in 2016. He received the Excellent Doctoral Dissertation Award from Peking University. He is serving as a Guest Editor for a Special Section of the IEEE ACCESS.

Binbin Ye received the B.S. and M.S. degrees from the South China University of Technology, Guangzhou, China, in 2013 and 2016, respectively. His research interests include index modulation and OFDM.

Ertugrul Basar (S'09–M'13–SM'16) received the B.S. degree (Hons.) from Istanbul University, Turkey, in 2007, and the M.S. and Ph.D. degrees from Istanbul Technical University in 2009 and 2013, respectively. From 2011 to 2012, he was with the Department of Electrical Engineering, Princeton University, Princeton, NJ, USA. He was an Assistant Professor with Istanbul Technical University from 2014 to 2017, where he is currently an Associate Professor of Electronics and Communication Engineering.

He is an inventor of two pending patents on index modulation schemes. His primary research interests include MIMO systems, index modulation, cooperative communications, OFDM, and visible light communications. He was a recipient of the Istanbul Technical University Best Ph.D. Thesis Award in 2014. He received three best paper awards, including one from the IEEE International Conference on Communications. He currently serves as an Associate Editor of the IEEE COMMUNICATIONS LETTERS and the IEEE ACCESS. He is also a regular reviewer for various IEEE journals, and has served as a TPC member for several conferences.

Qiang Li received the B.S. degree from the Inner Mongolia University of Science and Technology, Baotou, China, in 2013, and the M.S. degree from the Nanjing University of Aeronautics and Astronautics, Nanjing, China, in 2016. He is currently pursuing the Ph.D. degree with the South China University of Technology, Guangzhou, China. His recent research interests include MIMO systems, index modulation, and OFDM.

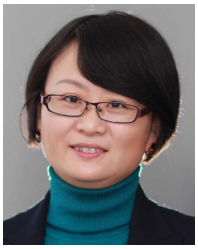

Fei Ji (M'06) received the Ph.D. degree from the South China University of Technology in 1998. She joined the South China University of Technology as a Lecturer. She was an Associate Professor from 2003 to 2008. She was with the City University of Hong Kong as a Research Assistant from 2001 to 2002 and a Senior Research Associate in 2005. She was with the University of Waterloo as a Visiting Scholar from 2009 to 2010. She is currently a full-time Professor with the South China University of Technology. Her research focuses on wireless communication systems and networking.